

1  
2  
3  
4  
5  
6  
7  
8  
9  
10  
11  
12  
13  
14  
15  
16  
17  
18  
19  
20  
21  
22  
23  
24  
25  
26  
27  
28  
29

**Sea ice break-up and freeze-up indicators for users  
of the Arctic coastal environment**

John E. Walsh<sup>1</sup>, Hajo Eicken<sup>1</sup>, Kyle Redilla<sup>1</sup>, Mark Johnson<sup>2</sup>

<sup>1</sup>International Arctic Research Center, University of Alaska Fairbanks, Fairbanks AK 99775  
USA

<sup>2</sup>College of Fisheries and Ocean Sciences, University of Alaska Fairbanks, Fairbanks AK  
99775 USA

*Correspondence to:* John E. Walsh (jewalsh@alaska.edu)

September 2022  
*The Cryosphere*, Revision 2

## Abstract

30

31 The timing of sea ice retreat and advance in Arctic coastal waters varies substantially from year  
32 to year. Various activities, ranging from marine transport to the use of sea ice as a platform for  
33 industrial activity or winter travel, are affected by variations in the timing of break-up and  
34 freeze-up, resulting in a need for indicators to document the regional and temporal variations in  
35 coastal areas. The primary objective of this study is to use locally-based metrics to construct  
36 indicators of break-up and freeze-up in the Arctic/Subarctic coastal environment. The indicators  
37 developed here are based on daily sea ice concentrations derived from satellite passive  
38 microwave measurements. The “day of year” indicators are designed to optimize value for  
39 users while building on past studies characterizing break-up and freeze-up dates in the open  
40 pack ice. Relative to indicators for broader adjacent seas, the coastal indicators generally show  
41 later break-up at sites known to have landfast ice. The coastal indicators also show earlier  
42 freeze-up at some sites in comparison with freeze-up for broader offshore regions, likely tied to  
43 earlier freezing of shallow water regions and areas affected by freshwater input from nearby  
44 streams and rivers. A factor analysis performed to synthesize the local indicator variations  
45 shows that the local break-up and freeze-up indicators have greater spatial variability than  
46 corresponding metrics based on regional ice coverage. However, the trends towards earlier  
47 break-up and later freeze-up are unmistakable over the post-1979 period in the synthesized  
48 metrics of coastal break-up/freeze-up and the corresponding regional ice coverage. The findings  
49 imply that locally defined indicators can serve as key links between pan-Arctic or global  
50 indicators such as sea-ice extent or volume and local uses of sea ice, with the potential to inform  
51 community-scale adaptation and response.

52 *Key words:* sea ice, Arctic, break-up, freeze-up, ice concentration

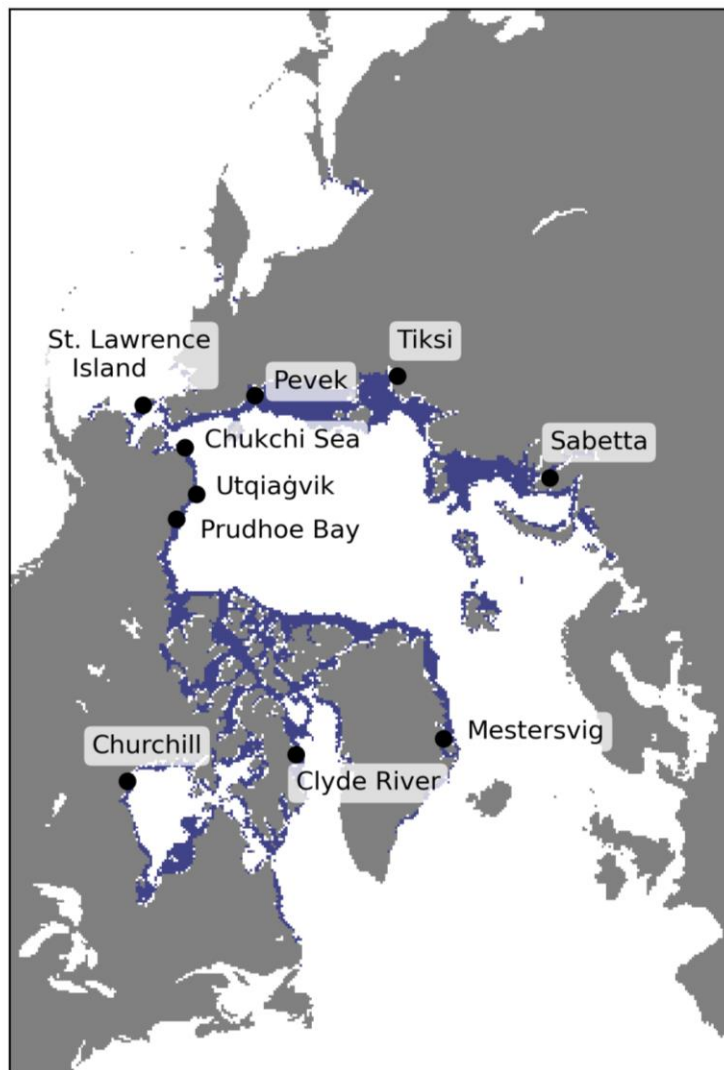
53 **1. Introduction**

54 Coastal sea ice impacts residents and other users of the nearshore marine environment in  
55 various ways. Perhaps most obvious is the fact that non-ice strengthened vessels require ice-  
56 free waters for marine transport, which can serve purposes such as resupply of coastal  
57 communities, the transport of extracted resources (oil, liquefied natural gas, mined metals),  
58 migration of marine mammals (e.g., bowhead whales) and wintertime travel over the ice by  
59 coastal residents. Key metrics for such uses of the nearshore marine environment are the  
60 timing of break-up (or ice retreat) in the spring and the timing of freeze-up (or ice advance) in  
61 the autumn or early winter.

62 Sea ice concentration thresholds have been used in various studies to determine the dates of  
63 sea ice opening, retreat, advance and closing (Markus et al., 2009; Johnson and Eicken, 2016;  
64 Bliss and Anderson; 2018; Peng et al., 2018; Bliss et al., 2019; Smith and Jahn, 2019). An  
65 emerging tendency in these and similar studies is the definition of break-up date as the date on  
66 which ice concentration drops below a prescribed threshold and remains below that threshold  
67 for a prescribed minimum duration (chosen to eliminate repeated crossings of the  
68 concentration threshold as a result of temperature- or wind-driven changes in ice coverage in  
69 response to transient weather events). A corresponding criterion is used for the freeze-up date.

70 Coastal regions present special challenges in the application of such criteria. First, landfast or  
71 shorefast ice (stationary sea ice held in place along the shoreline as a result of grounding  
72 and/or confinement by the coast) is common in waters immediately offshore of the coast,  
73 particularly in areas with shallow water. Landfast ice provides especially important sea ice  
74 services because it offers a stable platform for nearshore travel, serves as a critical habitat for  
75 marine mammals such as seals and polar bears (Dammann et al., 2018), and provides a buffer

76 against coastal storms (Hosekova et al., 2021). Landfast ice extends offshore by hundreds of  
77 meters to many tens of kilometers. Figure 1 shows the geographical distribution of landfast ice  
78 in terms of the maximum extent during June for the period 1972-2007. Landfast ice is most  
79 extensive over shallow waters of the Siberian Seas and the Canadian Archipelago. Given its  
80 widespread presence at coastal sites in the Arctic, landfast ice will be a key feature in our  
81 assessment of any differences in the sea-ice indicators, particularly for ice break-up, when  
82 comparing coastal to offshore regions.



84 Figure 1. Landfast ice distribution shown as the maximum extent of landfast ice over the  
85 1972-2007 period. Data source: National Ice Center via National Snow and Ice Data Center,  
86 NSIDC dataset G02172 -- <https://nsidc.org/data/G02172> (accessed 4 September 2022).

87 A second challenge associated with coastal regions is that sea ice concentrations derived from  
88 passive microwave measurements are prone to contamination by microwave emissions from  
89 land in coastal grid cells. Additionally, many parts of the Arctic coastline have inlets, river  
90 deltas and barrier islands that are not captured by the 25 km resolution of the passive  
91 microwave product. While higher-resolution datasets permitting finer resolution of coastal sea  
92 ice are available from sensors such as AMSR (Advanced Microwave Scanning Radiometer),  
93 the record lengths are sufficiently shorter (about 20 years for AMSR) that trend analyses are  
94 limited by a reliance on such products. Trend analysis is one of the main components of the  
95 present study.

96 A pervasive finding from recent studies of trends in Arctic sea ice is a shortening of the sea  
97 ice season. This finding is often presented in terms of the corresponding lengthening of the  
98 open water season (e.g., Stroeve et al., 2014; Stroeve and Notz, 2018; Onarheim et al., 2018;  
99 Bliss and Anderson, 2018; Peng et al., 2019; Smith and Jahn, 2019). Because the reduction of  
100 ice extent has been greater in summer than in winter, the percentage of the Arctic sea ice  
101 cover experiencing break-up and freeze-up (i.e., the percentage of the maximum ice cover that  
102 is seasonal) has increased from about 50% in 1980 to more than 70% in recent years  
103 (Druckenmiller et al., 2021; Thomson et al., 2022). Since 1980, the length of the open water  
104 period has increased by between one and two months (over 10 days per decade)  
105 (Stammerjohn et al., 2012; Peng et al., 2019; Thomson et al., 2022), with contributions of  
106 comparable magnitude from earlier break-up and later freeze-up. Regional variations of these

107 trends, both in the vicinity of the coasts and in regions farther offshore, are the focus of this  
108 paper as well as Bliss et al. (2019), to which we will compare our results.

109 Trends in freeze-up have been shown previously to be sensitive to the criterion for freeze-up  
110 (Peng et al., 2018; Bliss et al., 2019). For example, Peng et al. (2018) found that the trends in  
111 the autumn crossing of the 80% concentration were greater than trends in the crossing of the  
112 15% threshold (Thomson et al., 2022), implying a slowing of the autumn/winter ice advance.  
113 Such findings, as well as those of Johnson and Eicken (2016), motivate our use of separate  
114 indicators for the start and end of break-up and freeze-up.

115 The delayed autumn freeze-up is a manifestation of the release of increased amounts of heat  
116 stored in the upper layers of the ocean, largely as a result of the increased solar absorption  
117 made possible by the earlier break-up. In this respect, trends in break-up and freeze-up are  
118 intertwined. This linkage has been demonstrated quantitatively by Serreze et al. (2016) and  
119 Stroeve et al. (2016), who explored the use of break-up timing as a predictor of the timing of  
120 ice advance in the Chukchi Sea and the broader Arctic, respectively.

121 The primary objective of this study is to use the locally-based metrics to construct indicators  
122 of break-up and freeze-up on Arctic/Subarctic coastal environments. A secondary objective is  
123 to contribute to efforts at the national and global scale to establish key sets of indicators that  
124 support sustained assessment of climate change and inform planning and decision-making for  
125 adaptation action (AMAP, 2018; IPCC, 2022). At the global, pan-Arctic, and U.S. national  
126 levels, indicators associated with the state of the sea ice cover so far have focused on the  
127 summer minimum and winter maximum extent and ice thickness (IPCC, 2022; AMAP, 2017;  
128 Box et al., 2019; USGCRP, 2017). As outlined by Box et al. (2019), this approach has been  
129 motivated by the objective of describing and tracking the state of key components of the

130 global climate system. However, large-scale (pan-Arctic) measures of e.g., sea-ice extent or  
131 volume are of little value and relevance to those needing to adapt or respond to such change at  
132 the community or regional scale. Here, we examine the timing of sea-ice freeze-up and break-  
133 up as key constraints for a range of human activities and ecosystem functions in Arctic  
134 settings.

## 135 **2. Data and methods**

136 The primary data source is the archive of gridded daily sea ice concentrations derived from  
137 the SMMR, SSM/I and SSMIS sensors onboard the Nimbus-7 and various DMSP satellites  
138 dating back to November, 1978. The dataset is NSIDC-0051 of the National Snow and Ice  
139 Data Center (NSIDC) and is accessible at <https://nsidc.org/data/nsidc-0051>. In the  
140 construction of this dataset, the NASA Team algorithm (Cavalieri et al., 1984) was used to  
141 process the microwave brightness temperatures into a consistent time series of daily sea ice  
142 concentrations. The data are on a polar stereographic grid projection with a grid cell size of 25  
143 km x 25 km. Prior to computing the break-up and freeze-up metrics described below, the data  
144 were processed with a linear interpolation to fill in missing daily values, followed by a spatial  
145 and then temporal smoothing to filter out short (< 3 days) events. Specifically, the daily sea  
146 ice concentration values were spatially smoothed using a generic boxcar filter with a square  
147 footprint of 3 x 3 grid cells. The data were then temporally smoothed three times using a Hann  
148 window.

149 The daily sea ice concentrations are used to define the metrics of the start and end of break-up  
150 and freeze-up in each year of a 40-year period, 1979-2018. The definitions build on those  
151 used by Johnson and Eicken (2016; hereafter denoted as J&E), which were informed by  
152 Indigenous experts' observations of ice use and ice hazards in coastal Alaska, and relate to

153 planning and decision-making at the community-scale (Eicken et al., 2014). Here, we expand  
154 the satellite data analysis with minor modifications of the break-up and freeze-up criteria to  
155 broaden the applicability to coastal areas. Examples include imposing maximum and  
156 minimum values for the thresholds computed from summary statistics of the daily sea ice  
157 concentration values of relevant periods. The revised definitions are presented in Table 1 and  
158 the differences relative to those of J&E are listed in Table 2.

159 The four indicators in this study are the dates of the start and end of break-up and freeze-up.  
160 For purposes of this study, the break-up period may be regarded as the time between the  
161 Arctic sea ice maximum (typically in March) and the sea ice minimum (typically in  
162 September, with June representative of the period most rapid break-up). Similarly, the freeze-  
163 up period extends from September through March, with November representative of the  
164 period of most rapid freeze-up. The corresponding indicators used by Bliss et al. (2019) are  
165 the date of opening (defined as the last day on which the ice concentration drops below 80%  
166 before the summer minimum), the date of retreat (defined as the last day the ice concentration  
167 drops below 15% before the summer minimum), the date of advance (defined as the first day  
168 the ice concentration increases above 15% following the final summer minimum) and the date  
169 of closing (defined as the first day the ice concentration increases above 80% following the  
170 final summer minimum). For the comparisons of indicator dates presented in Section 3, we  
171 did not make any modifications to the Bliss et al. (2019) criteria.

172 While the various thresholds in Table 1 may seem somewhat arbitrary at first glance, they are  
173 based on past sensitivity tests. In particular, the 10% threshold is based on prior work (J&E)  
174 in which sensitivities were explored. The selected thresholds were those that generally  
175 maximized the number of such years across the coastal locations and MASIE regions.



176  
177  
178  
179  
180  
181  
182  
183  
184  
185  
186  
187  
188  
189  
190  
191  
192  
193  
194  
195  
196  
197

Table 1. Definition of the start and end of break-up and freeze-up.

**Break-up start** The date of the last day for which the previous two weeks' ice concentration always exceeds a threshold computed as the maximum of (a) the winter (January-February) average minus two standard deviations and (b) 15%. Undefined if the average summer sea ice concentration (SIC) is greater than 40% or if the subsequent break-up end is not defined.

**Break-up end** The first date after the break-up start date for which the ice concentration during the following two weeks is less than a threshold computed as the maximum of (a) the summer (August-September) average plus one standard deviation and (b) 50%. Undefined if the daily SIC is less than the threshold for the entire summer or if break-up start is not defined.

**Freeze-up start:** The date on which the ice concentration exceeds for the first time a threshold computed as the maximum of (a) the summer (August-September) average plus one standard deviation and (b) 15%. Undefined if the daily SIC never exceeds this threshold, if the mean summer SIC is greater than 25%, or if subsequent freeze-up end is not defined.

**Freeze-up end:** The first date after the freeze-up start date for which the following two weeks' ice concentration exceeds a threshold computed as the maximum of (a) the average winter (January-February) ice concentration minus 10% and (b) 15%, and the minimum of this result and (c) 50%. Undefined if daily SIC exceeds this threshold for every day of the search period or if freeze-up start is not defined.

198 Table 2. Changes in the indicator definitions relative to Johnson and Eicken (2016), denoted  
199 as “J&E”. The symbol “ $\sigma$ ” denotes standard deviation; “sic” denotes sea ice concentration.

200 *Break-up start:*

201 - minimum sic threshold created at 15% (J&E: last day exceeding Jan-Feb mean minus  $2\sigma$ )

202 - undefined if average summer sic > 40% (J&E: no such criterion)

203 - undefined if subsequent breakup end date not defined (J&E: no such criterion)

204

205 *Break-up end:*

206 - first time sic below threshold for 2 weeks instead of last day below threshold

207 (J&E: last exceeding larger of Aug-Sep mean or 15%)

208 - minimum threshold 50% (J&E: minimum threshold of 15%)

209 - undefined if break-up start not defined (J&E: no such criterion)

210

211 *Freeze-up start:*

212 - first day on which sic exceeds Aug-Sep average by  $1\sigma$  (J&E: same)

213 - undefined if mean summer sic > 25% (J&R: no such criterion)

214 - undefined if subsequent freeze-up end not defined (J&E: same)

215

216 *Freeze-up end:*

217 - first time sic above threshold for following 2 weeks instead of first day above threshold

218 (threshold is Jan-Feb average minus 10%, as in J&E)

219 - thresholds imposed: Minimum (15%) and maximum (50%) (J&E: no such thresholds)

220 - undefined if sic always exceeds threshold (J&E: same)

221 Our evaluation of the coastal indicators includes comparisons of the various dates (break-  
222 up/freeze-up start/end) at nearshore locations with the corresponding metrics for broader areas  
223 of the Arctic Ocean and the subarctic seas. A set of ten locations was selected on the basis of  
224 their geographical distribution and the relevance of local sea ice to uses by communities,  
225 industry, military or other stakeholders. Examples of local uses include over-ice travel for  
226 access to marine mammals, offshore travel between coastal communities, access of coastal  
227 facilities by commercial vessels, and protection from coastal waves and erosion. The ten  
228 locations are shown in Figure 2 and listed in Table 3, together with their geographic  
229 coordinates. While there is admittedly some subjectivity in the selection of these sites, our  
230 priorities were (1) a pan-Arctic geographical distribution, thereby expanding the emphasis on  
231 North American locations in past studies (see Discussion in Section 4) and (2) inclusion of  
232 locations with a mix of users affected by sea ice: Indigenous communities, industry, military  
233 and other stakeholders. For each of these locations, several passive microwave grid cells close  
234 to (but not adjacent to) the coastline were selected for calculation of the break-up and freeze-  
235 up metrics. More specifically, the contamination of the passive microwave-derived ice  
236 concentrations by the presence of land in a grid cell required the exclusion of grid cells  
237 containing land. Therefore, the selected grid cells satisfied the criterion that they were the  
238 cells closest to the coast but centered at least 25 km from the coast. Figure 2 shows  
239 geographical insets illustrating the proximity of the selected grid cells to the coastline.

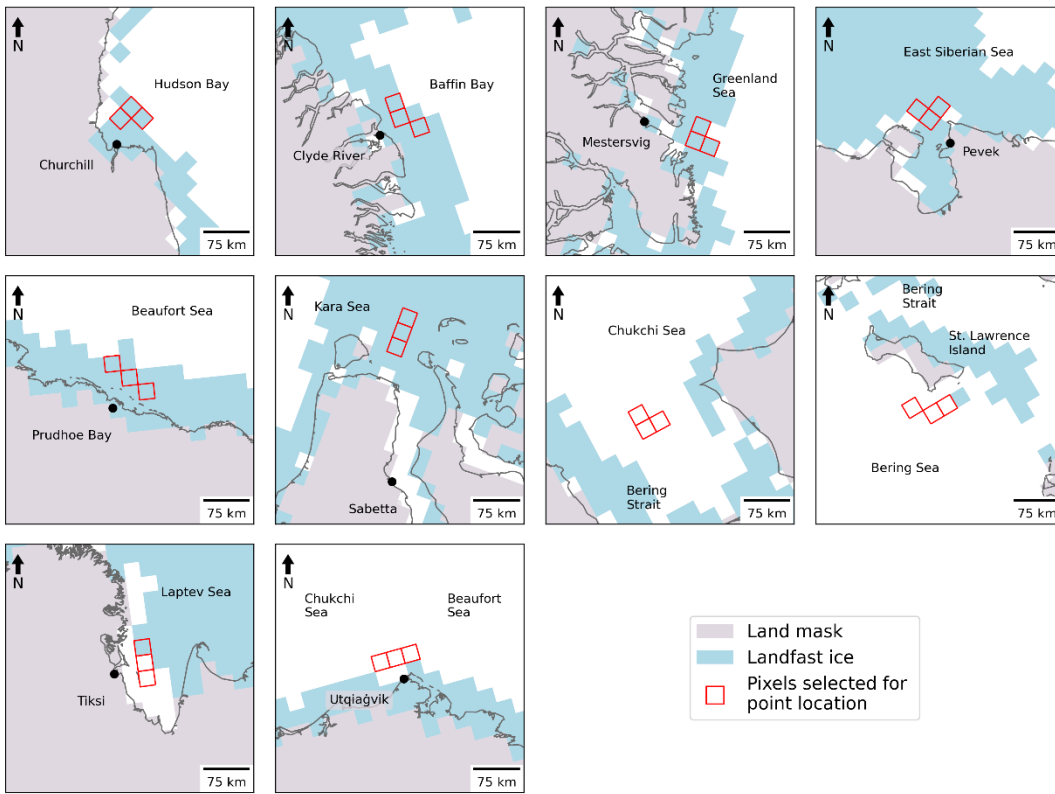
240 With regard to the grid cell selection, we experimented with the grid cell selections at Sabetta  
241 and Utqiagvik. When the grid cell locations were shifted offshore by one pixel at Sabetta, the  
242 mean break-up start and end dates changed by only -0.1 and -1.1 days, respectively; the  
243 corresponding changes in the freeze-up start and end dates were 0.2 and -0.7 days,

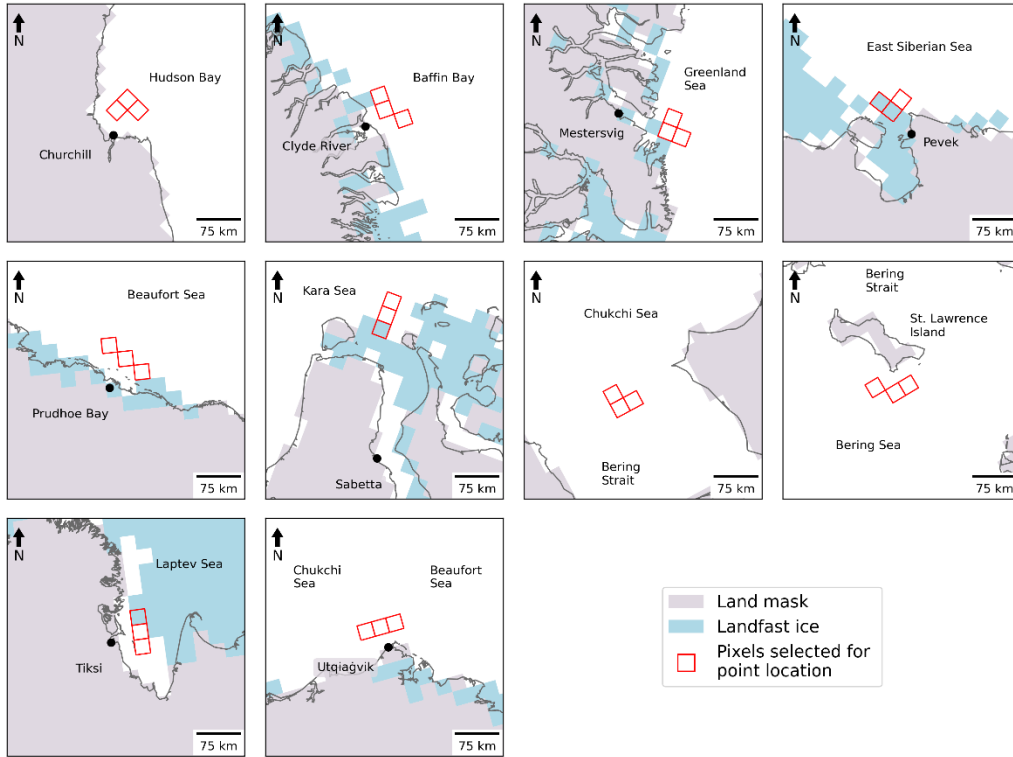
244 respectively. At Utqiagvik, the offshore shift resulted in an earlier mean break-up start by 3.3  
 245 days and a later mean break-up end by 2.9 days. The earlier break-up start is consistent with  
 246 the presence of landfast ice at the coast, as discussed in Section 4. The changes in Utqiagvik's  
 247 freeze-up dates were small when the pixels were shifted offshore, where the start of freeze-up  
 248 occurred 1.1 days later and the end of freeze-up 1.1 days earlier than closer to the coast.

249

250 Table 3. Near-coastal locations selected for calculation of break-up and freeze-up metrics

251	<u>Sea</u>	<u>Location</u>	<u>Latitude, Longitude</u>	<u>Significance of location</u>
252	Beaufort Sea	Prudhoe Bay	70.2N, 148.2W	oil facilities
253	Chukchi/Beaufort Seas	Utqiagvik	71.3N, 156.8W	Indigenous community
254	Chukchi Sea	Chukchi Sea	69.6N, 170W	shipping route
255	Bering Sea	St. Lawrence Island	65.7N, 168.4W	Indigenous community
256	East Siberian Sea	Pevek	69.8N, 170.6E	port, mining facility
257	Laptev Sea	Tiksi	71.7N, 72.1E	research site, port
258	Kara Sea	Sabetta	71.3N, 72.1E	port, LNG facility
259	Greenland Sea	Mestersvig	72.2N, 23.9W	military base
260	Baffin Bay	Clyde River	70.3N, 68.3W	Indigenous community
261	Hudson Bay	Churchill	58.8N, 94.2W	port, tourism





264

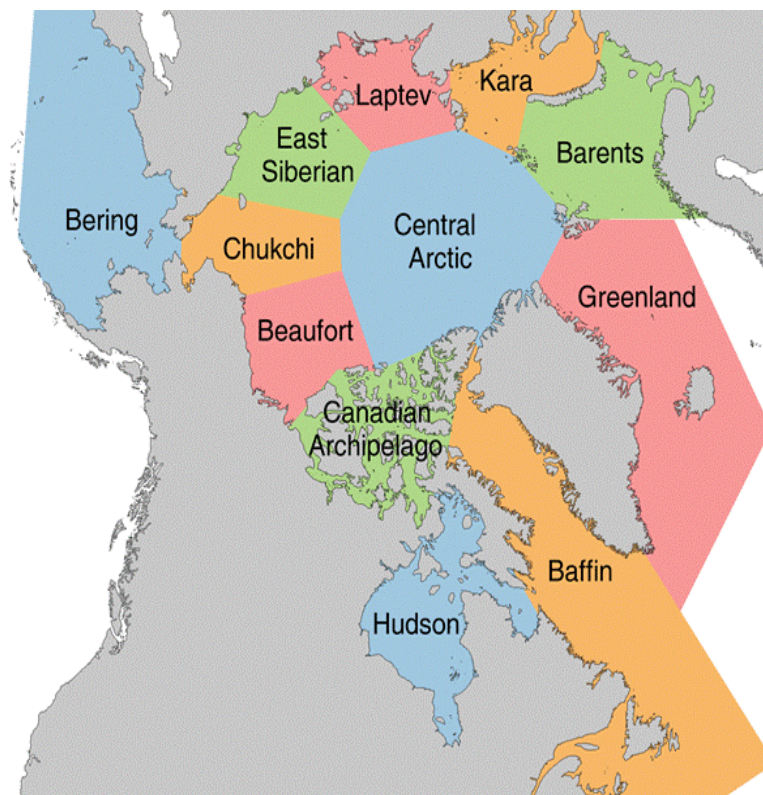
265 Figure 2. Grid cells (red squares) for which passive-microwave-derived ice concentrations  
 266 were used in computing the break-up and freeze-up metrics for the coastal locations. Black  
 267 dots represent the actual locations of the coastal communities. Blue shading denotes  
 268 maximum (upper panels) and median (lower panels) coverage of landfast ice in June over the  
 269 1972-2007 period based on charts of the U.S. National Ice Center --  
 270 <https://nsidc.org/data/G02172> (accessed 28 June 2022).

271 It is apparent from Figure 2 that the innermost extent of the landfast ice does not always  
 272 coincide with the coastline, which we assume here should always be the inner boundary of  
 273 landfast ice. The northern Siberian coast (Sabetta and Tiksi) provides examples. In pursuing  
 274 an explanation for the discrepancies, we found that the land mask in the landfast ice dataset  
 275 (digitized charts of the National Ice Center) differs from the land mask of the NSIDC's

276 passive microwave dataset. The resulting offset does not change the area covered by sea ice in  
277 each regional plot, but it does result in the mis-location of the inner boundary of landfast ice.  
278 The discrepancy does not alter the reasoning about the geographically varying roles of  
279 landfast ice, as discussed in Section 4, and a more detailed analysis of the origin of these  
280 offsets in coastline depiction and landfast ice location is beyond the scope of this paper.

281 The grid cell selections for St. Lawrence Island and the Chukchi Sea deserve special  
282 comment. The grid cells off St. Lawrence Island were chosen to reflect timing and location of  
283 subsistence harvests by the communities of Gambell and Savoonga. Because of extensive ice  
284 coverage, including landfast ice, north and northwest of the island, both communities  
285 traditionally conduct bowhead whale harvests at hunting camps on the south side of the island  
286 once spring ice break-up is underway (Noongwook et al., 2007). These sites also reflect the  
287 seasonal migration of whales in waters south of the island with the seasonal retreat of the ice  
288 cover (Noongwook et al., 2007), modulated somewhat by the presence of a polynya south and  
289 southwest of the island (Krupnik et al., 2010; Noongwook et al., 2007). Traditional walrus  
290 harvest practices on St. Lawrence Island await the very end of the bowhead whale hunt  
291 (Kapsch et al., 2010), with timing of spring ice break-up south of the island as the driving  
292 factor. These practices motivated our selection of grid cells southeast of the island. As shown  
293 later (Section 4), landfast ice is confined to the northern coastal region of St. Lawrence Island  
294 – consistent with the frequent presence of the polynya south of the island. In the case of the  
295 Chukchi Sea, the grid cells are indeed farther from the coast than for the other sites; the  
296 locations were intentionally selected to be farther offshore in order to provide a non-coastal  
297 counter-example to the other sites, all of which are adjacent to a coast.

298 Previous studies cited earlier have evaluated break-up and freeze-up metrics for subregions of  
299 the Arctic Ocean and the surrounding seas (Markus et al., 2006; Johnson and Eicken, 2016;  
300 Bliss and Anderson, 2018; Peng et al., 2018; Bliss et al., 2019; Smith and Jahn, 2019). For  
301 comparisons with broader regions offshore of our selected sites, we utilize the MASIE  
302 (Multisensor Analyzed Sea Ice Extent) regionalization  
303 ([https://nsidc.org/data/masie/browse\\_regions](https://nsidc.org/data/masie/browse_regions)). Of the MASIE regions shown in Figure 3, we  
304 choose the following for computation of regionally averaged metrics of break-up and freeze-  
305 up: Beaufort Sea, Chukchi Sea, East Siberian Sea, Laptev Sea, Kara Sea, Greenland Sea,  
306 Baffin Bay, Hudson Bay, and Bering Sea.



307

308 Figure 3. The MASIE subregions of the Arctic. Regions utilized in this study include  
309 Beaufort Sea, Chukchi Sea, East Siberian Sea, Laptev Sea, Kara Sea, Baffin Bay, Hudson  
310 Bay, and Bering Sea.

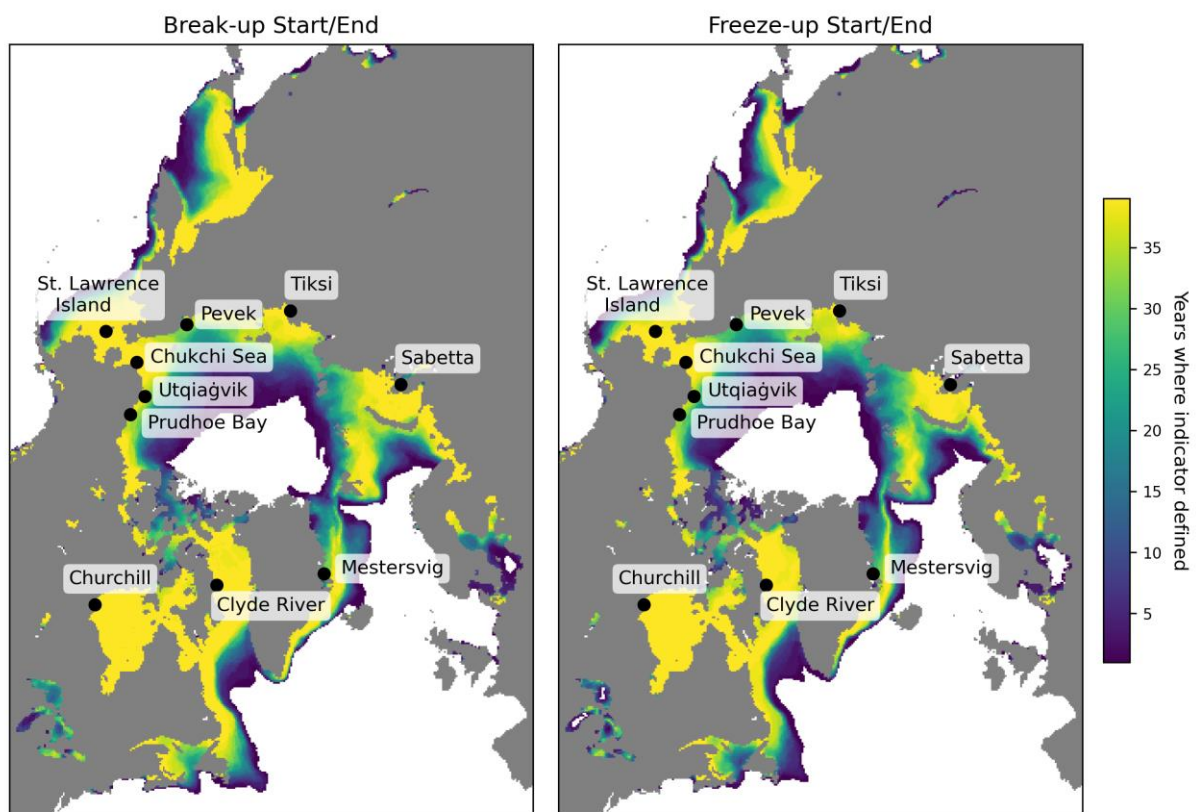


311 The following section includes time series of the local indicators and, for comparison, time  
312 series of the corresponding MASIE regional indicators. In order to address the spatial  
313 coherence of the indicators, we performed a factor analysis on the different sets (break-  
314 up/freeze-up, start/end dates). The computation of the indicators was done for the ten local  
315 sites and for the MASIE regions in which they fall. Factor analysis is a statistical method for  
316 quantifying relationships among a set of variables. The variability in the overall dataset is  
317 depicted by a set of factors. Each factor explains a percentage of the total variance in space  
318 and time. Each variable in each factor is given a loading (or weight) based on its contribution  
319 to the variance explained by that factor. The first factor can be viewed as the linear  
320 combination of the variables that maximizes the explained variance in the overall dataset. The  
321 second and each successive factor maximize the variance unexplained by the preceding  
322 factors. Successive factors explain successively smaller fractions of the overall variance.  
323 Multiple variables can have strong loadings in the same factor, indicating they follow a  
324 similar pattern and are likely highly related. Factor analysis has a long history of applications  
325 to Arctic sea ice variability (Walsh and Johnson, 1982; Fang and Wallace, 1994; Deser et al.,  
326 2000; Fu et al., 2021). The factor analysis calculations used here were performed using the  
327 XLSAT software package run in Excel (<https://www.xlstat.com/en/>)

### 328 **3. Results**

329 With coastal ice retreat and onset of ice advance as this study's primary foci, we first  
330 demonstrate the applicability of the indicators evaluated here. The various metrics of sea ice  
331 break-up and freeze-up in Table 1 are not defined for all locations in the Arctic. For example,  
332 locations that remain ice-covered throughout a particular year will not be assigned dates for  
333 any of the indicators in that year, and the same is true of locations at which sea ice does not

334 form during a particular year. Figure 4 shows the number of years in the 1979-2018 study  
335 period during which the break-up and freeze-up indicators are actually defined. It is apparent  
336 that the indicators are consistently defined in the seasonal sea ice zone spanning the subarctic  
337 seas. In particular, all ten coastal locations in Table 2 are in the yellow areas (>35 years out of  
338 40 years defined) of Figure 4. Of note in Figure 4 is that the number of years with defined  
339 break-up indicators slightly exceeds (by one) the number of years with freeze-up indicators at  
340 some locations at the outer periphery of the seasonal sea ice zone. These are locations in  
341 which sea ice was present for some portion of the early years but not at the end of the study  
342 period, so in one of the years there was a break-up but no freeze-up.



343

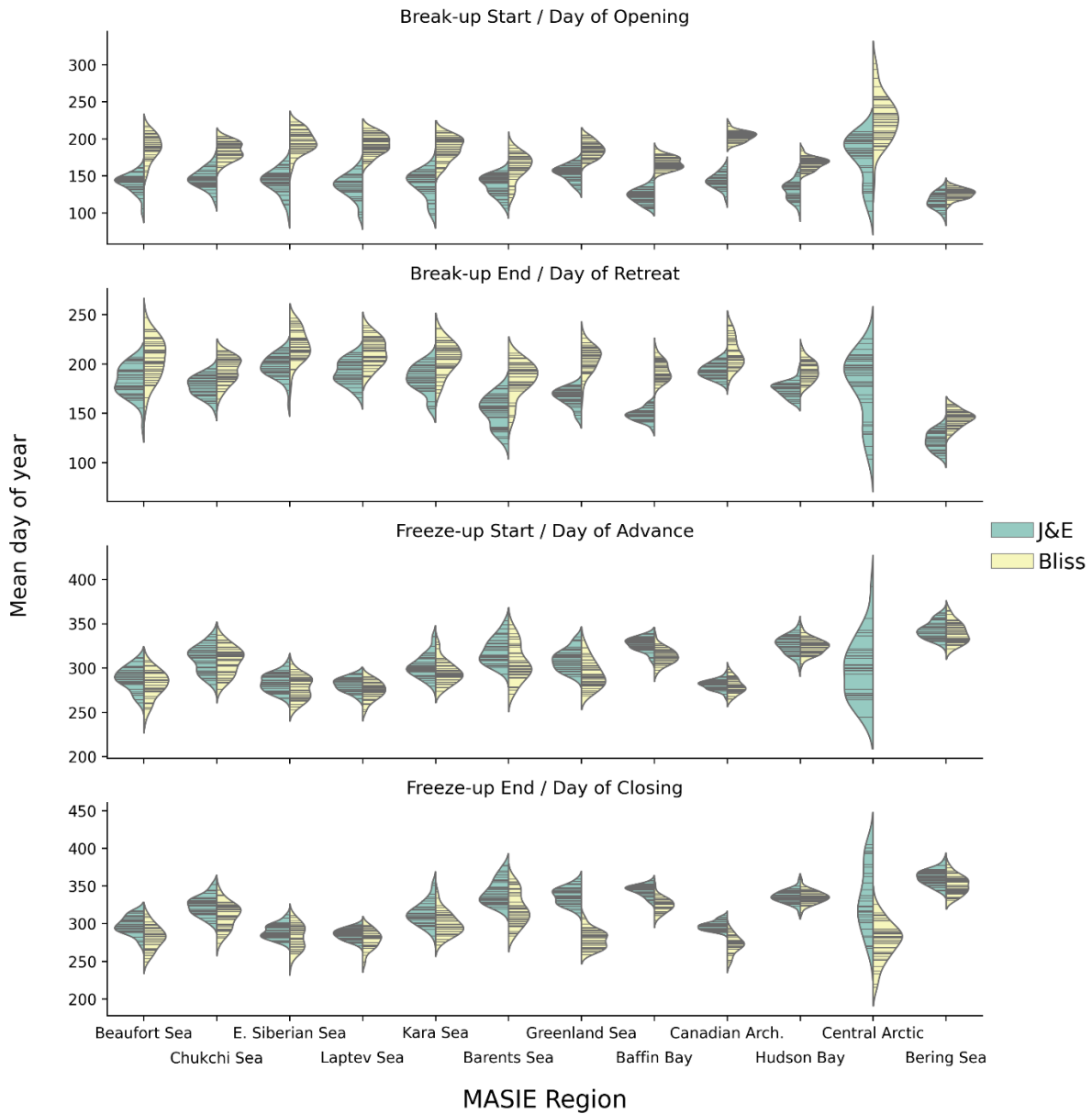
344 Figure 4. Number of years in the 1979-2018 study period in which the break-up and freeze-up  
345 indicators were defined. Note that end dates for break-up and freeze-up exist only for years in

346 which there are start dates for break-up and freeze-up. The start and end dates of the overall  
347 data record (1 Jan 1979 – 31 Dec 2018) can result in differences of 1 year in the counts when  
348 freeze-up occurs around January 1.

349

350 A key issue to be addressed is the degree to which the indicators utilized here differ from  
351 those of previous studies. The metrics of Bliss et al. (2019) or similar variants have been used  
352 in recent publications and provide natural points of comparison. While there are various  
353 differences between our metrics and those of Bliss et al., the most consequential for the  
354 computed dates is the use of departures from winter/summer averages concentrations in our  
355 criteria vs. Bliss et al.'s use of 15% and 80% concentrations as key thresholds. This  
356 distinction is analogous to the difference between the NASA Team algorithm's use of fixed  
357 tie points and the NASA Bootstrap algorithm's use of "dynamic" (time/space-varying) tie  
358 points.

359 Figure 5 and Table S1 show that there are systematic differences between our metrics (based  
360 on the modified J&E criteria) and those of Bliss et al. when the two sets of metrics are  
361 evaluated for the MASIE regions. In particular, J&E's start and end of breakup generally  
362 occur earlier by up to several weeks than the corresponding dates of opening and retreat  
363 defined by Bliss et al. On the other hand, J&E's freeze-up dates are more closely aligned with  
364 those of Bliss et al., although J&E's end-of-freeze-up occurs later (by 1 to 3 weeks) than Bliss  
365 et al.'s closing date in most of the MASIE regions, especially the North Atlantic and Canadian  
366 regions.



368

369 Figure 5. “Violin” plots of the Julian dates of the break-up/freeze-up metrics used in this  
 370 study based on Johnson and Eicken (2016) (green shading) and the corresponding dates of ice  
 371 opening, retreat, advance and closing as defined by Bliss et al. (2019) (yellow shading). A  
 372 violin plot shows a distribution by widening the horizontal lines in the ranges (of day of the  
 373 year, in this case) having the highest concentration of values. The thin black lines represent

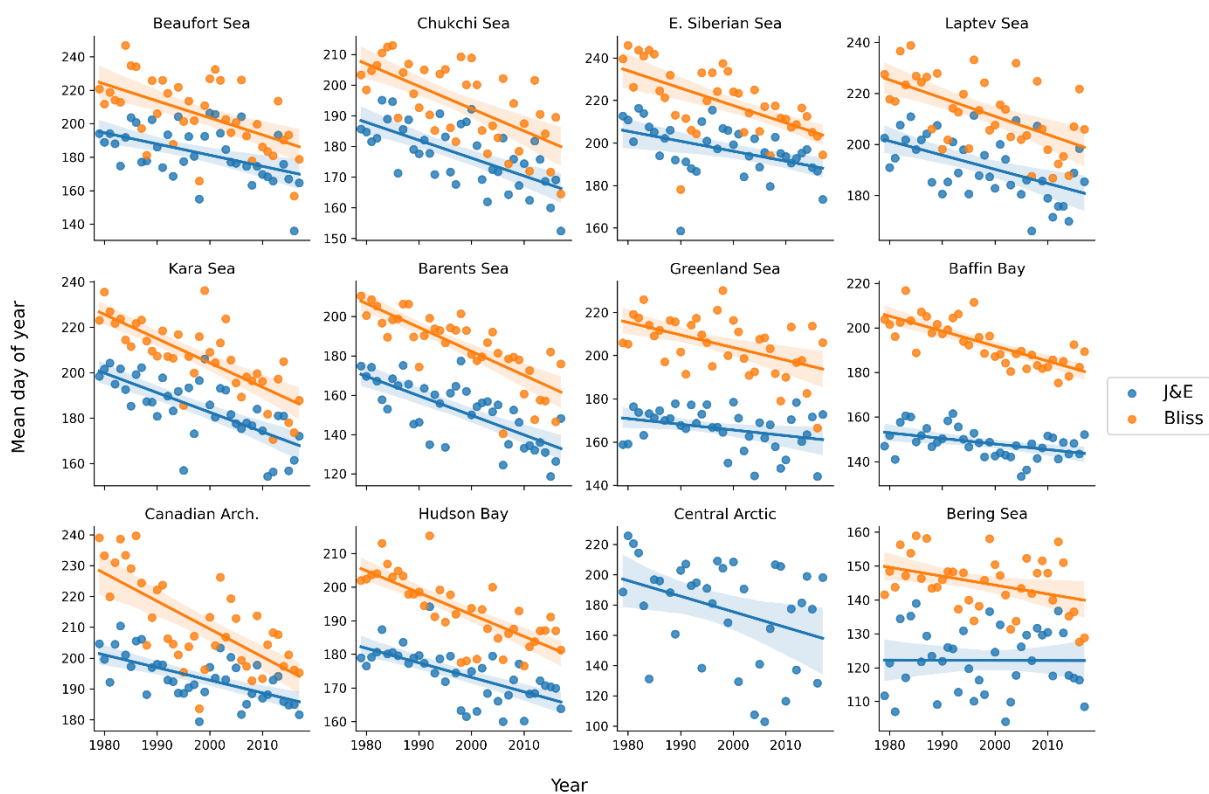
374 the observations themselves; the black strips are clusters of lines representing groups of  
375 similar values in the distribution. The violin plots provide no information about the temporal  
376 sequence of the values.

377 The violin plots in Figure 5 show distributions but not the temporal variations that have been  
378 indicated by results of previous studies (Peng et al., 2018; Bliss et al., 2019). Figures 6 and 7  
379 provide the temporal perspective on the end dates of break-up (Day of retreat) and freeze-up  
380 (Day of closing), respectively. In each of the MASIE regions, the J&E criterion gives an  
381 earlier break-up date. The difference is typically two to three weeks, although it exceeds a  
382 month in the Greenland Sea and Baffin Bay. Despite the offsets, the trends are nearly the  
383 same in nearly all the regions. Exceptions are the Canadian Archipelago, where the J&E trend  
384 is weaker than the Bliss trend, and the Bering Sea, where the trends are opposite in sign.  
385 However, the trend in the Bering region is not statistically significant at the 99% level by  
386 either metric, in contrast to all other regions in which the trends are significant at this level  
387 (Table S2). The main conclusion from Figure 6 is that, except for the Bering Sea, sea ice  
388 break-up is occurring earlier throughout the Arctic than several decades ago, no matter which  
389 metric is used.

390 In contrast to the trends towards earlier breakup, the J&E and Bliss metrics for the end of  
391 freeze-up both show significant trends towards later dates in most of the MASIE regions  
392 (Figure 7 and Table S3). In this case, even the Bering Sea shows a trend towards later freeze-  
393 up. Again, there is an offset towards a later date with the J&E metric, although the offset has  
394 a range among the regions, from essentially zero in Hudson Bay to more than six weeks in the  
395 Greenland Sea. The trends, however, show less agreement in some regions than do the trends  
396 for break-up dates in Figure 6. The J&E trends are less positive than the Bliss trends in the

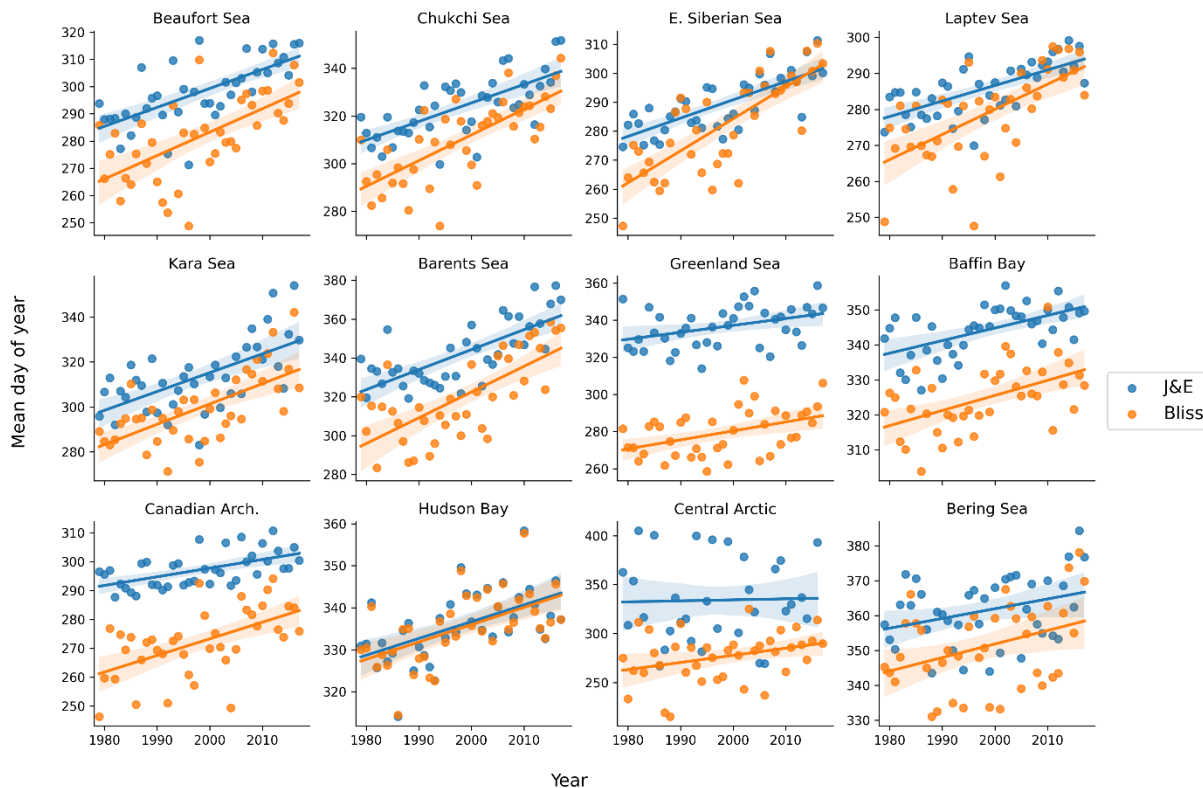
397 seas of the eastern Russian sector: the Chukchi, East Siberian and Laptev Seas. The same is  
 398 true, although to a lesser degree, in the Barents Sea and the Canadian Archipelago. The main  
 399 message from Figure 7 is that the freeze-up is ending later throughout the Arctic, although the  
 400 magnitude of the trend is more sensitive to the criteria used for end-of-freeze-up than for end-  
 401 of-break-up.

402



403

404 Figure 6. Yearly values of J&E’s break-up end date (blue symbols) and the Bliss et al.’s  
 405 (2019) Day of retreat (orange symbols) in the various MASIE regions. Corresponding trend  
 406 lines are shown in each panel. (For the Central Arctic region, Bliss et al.’s “Day of retreat”  
 407 metric is not shown because it was defined for fewer than half the years). Y-axis labels  
 408 represent day of the year. Date scales on y-axis vary among panels in order to optimize  
 409 display of data points. For numerical values of slopes and significance levels, see Table S2.



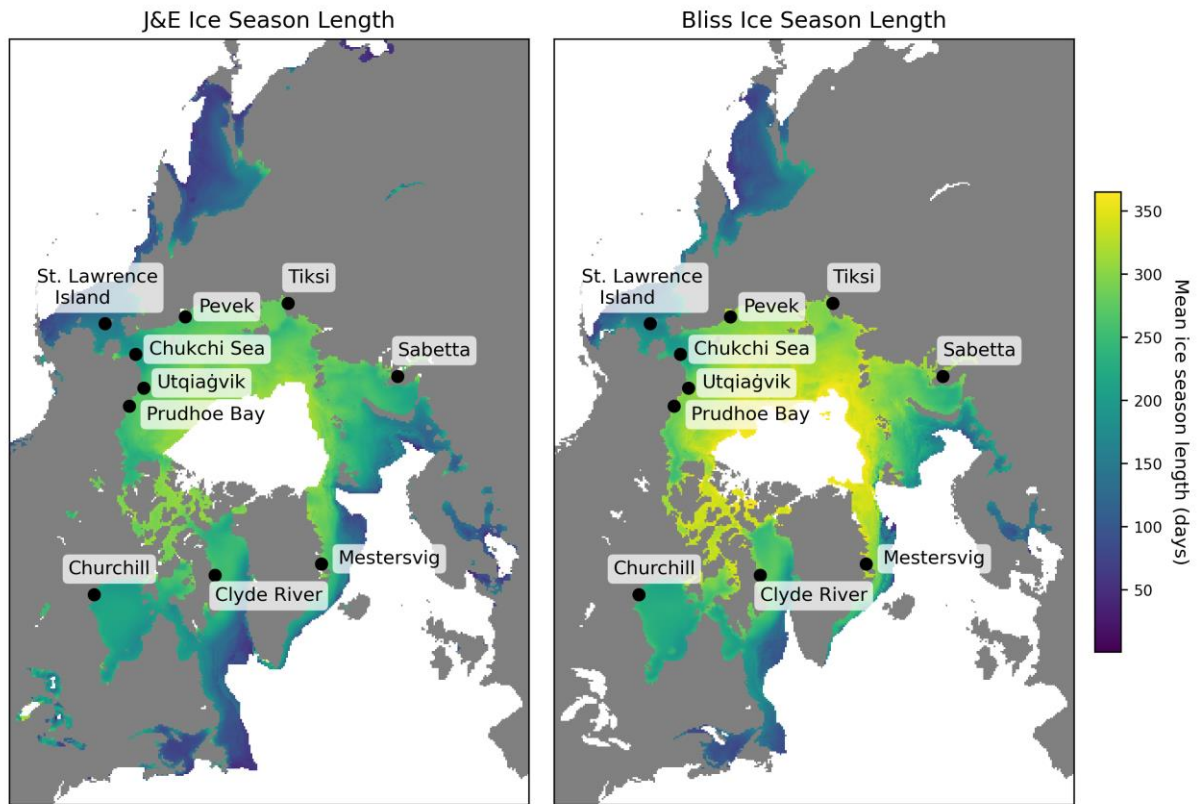
411

412 Figure 7. Yearly values of J&E’s freeze-up end date (blue symbols) and the Bliss et al.’s  
 413 (2019) Day of closing (orange symbols) in the various MASIE regions. Corresponding trend  
 414 lines are shown in each panel. Y-axes labels represent day of the year. Date scales on y-axis  
 415 vary among panels in order to optimize display of data points. Numerical values of slopes and  
 416 their significance levels are provided in Table S3.

417

418 A final comparison is presented in Figure 8, which shows the ice season lengths computed  
 419 using the two sets of metrics. The ice season length is defined as the number of days between  
 420 the end of freeze-up and the start of break-up. Consistent with J&E’s earlier break-up (Figure  
 421 6) and later freeze-up (Figure 7), the J&E metrics yield a shorter ice season than the Bliss et al  
 422 metrics. The differences in Figure 8 exceed a month in most of the Arctic except for the

423 Bering Sea, Hudson Bay and the Canadian Archipelago. However, the negative trends of ice  
424 season length are similar in magnitude according to both sets of metrics over most of the  
425 Arctic. The trend maps are not shown here because they add little to the information conveyed  
426 in Figures 6 and 7.



428 Figure 8. Mean ice season length based on the J&E metrics (left) and the Bliss et al. (2019)  
429 metrics (right). Metrics of break-up and freeze-up were not defined in a sufficient number of  
430 years in the white area near the North Pole.

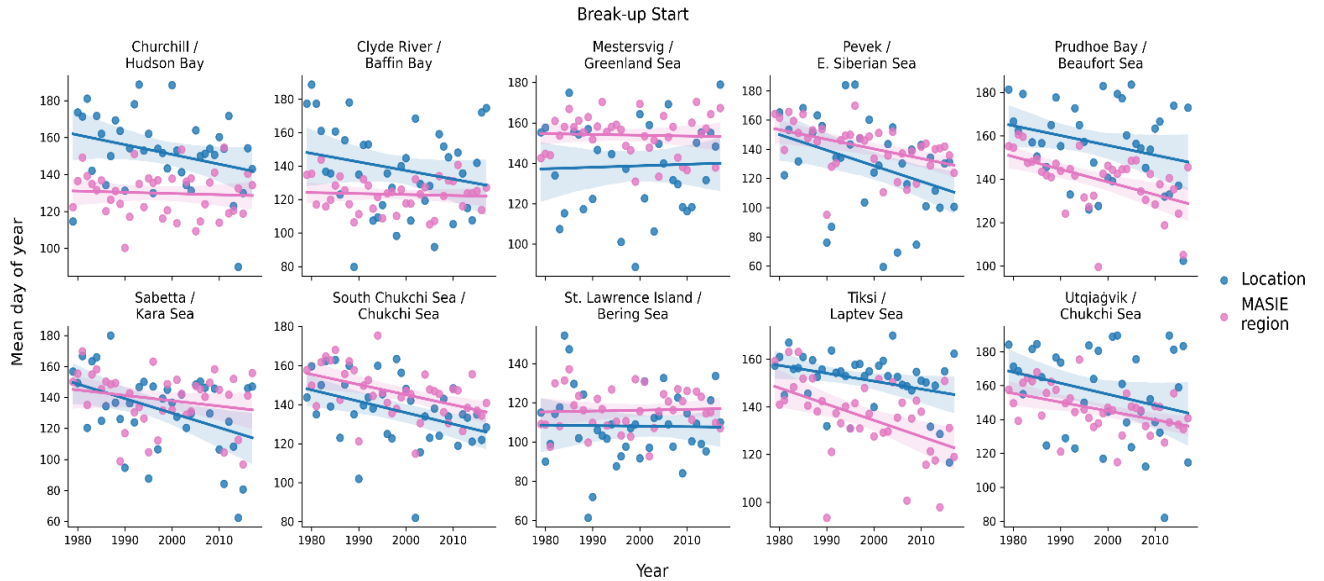
431 Given that this study targets the use of local indicators, it is important to assess the  
432 relationship between the local indicators and those for the broader MASIE regions containing  
433 the coastal locations. An important caveat in such a comparison is that our local indicators



434 were designed for coastal users, not for broader regional or applications in areas far from  
435 shore. This distinction introduces the possibility that the coastal indicators may be less than  
436 optimal for the larger MASIE regions. Figures 9-10 provide these comparisons for the break-  
437 up metrics defined by the modified J&E algorithms. In all cases, the yearly values (and linear  
438 trend lines) for the ten coastal locations in Table 3 are plotted for the 1979-2018 period,  
439 together with the values for the corresponding MASIE regions.

440 The break-up start dates (Figure 9) differ between the coastal locations and the broader  
441 MASIE regions in most of the ten cases, and in some cases the trends are notably different.  
442 With regard to systematic differences, not only the magnitude but also the sign of the offsets  
443 varies among the regions. The break-up start date at the coast is later than for the MASIE  
444 regions for Prudhoe (Beaufort Sea), Utqiagvik (Chukchi Sea), Tiksi (Laptev Sea), and both  
445 Canadian locations: Churchill (Hudson Bay) and Clyde River (Baffin Bay). These sites are all  
446 Arctic coastal locations at which varying extents of landfast ice are present. By contrast, the  
447 coastal locations have earlier break-up start dates (relative to their corresponding MASIE  
448 regions) at St. Lawrence Island, Mestersvig (Greenland Sea) and the Bering Strait (Chukchi  
449 Sea. The relation of landfast ice to the timing of break-up is discussed further in Section 4.

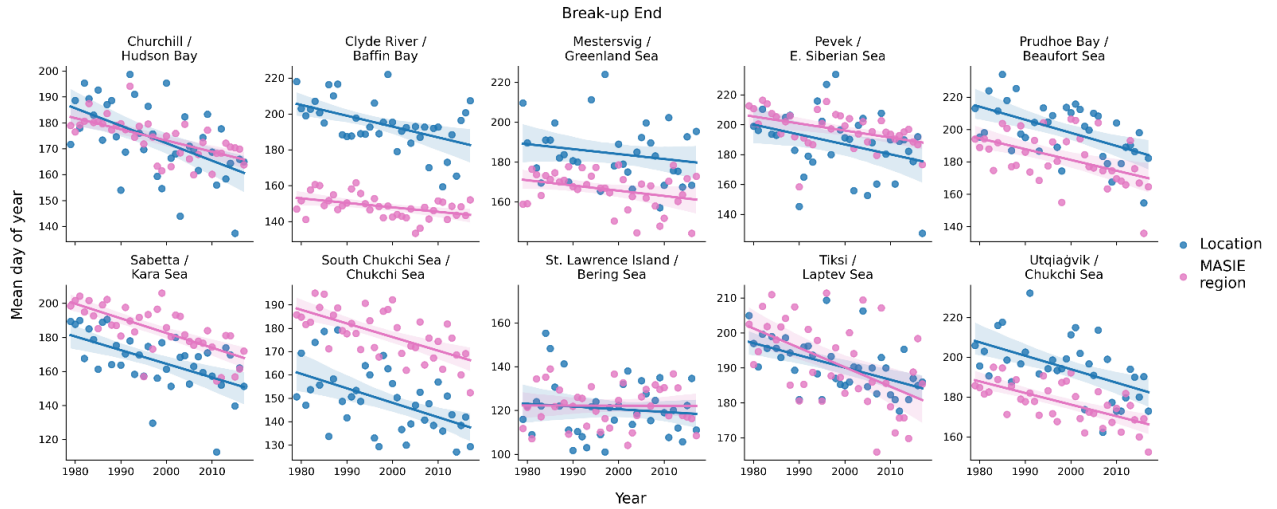
450 While the general trend towards earlier break-up noted above (Figure 6) is apparent at most of  
451 the coastal locations, the magnitudes of the trends can differ between the coastal sites and the  
452 broader MASIE regions. Figure 9 shows that the trend towards an earlier start of break-up is  
453 stronger at the coastal location relative to the MASIE region at Churchill, Clyde River, Pevek  
454 and Sabetta. Only at Tiksi is the negative trend weaker at the coastal site. In the other regions  
455 the trends are nearly identical.



456

457 Figure 9. Yearly values (1979-2018) of the break-up start dates (shown as day-of-the-year numbers)  
 458 for the coastal locations (blue) and the corresponding MASIE regions (pink). Date scales on y-axis vary  
 459 among panels in order to optimize display of data points. Linear regression lines are shown with the  
 460 same color coding. In each panel, the upper line of header identifies the coastal location and the lower  
 461 line identifies the MASIE region. All values are based on the modified J&E algorithms. Slopes and  
 462 their significance levels are listed in Tables S2 and S3.

463 The break-up end dates (Figure 10) show differences similar to those in Figure 9 in most, but  
 464 not all, cases. The break-up end date occurs later at Clyde River, Prudhoe and Utqiagvik  
 465 relative to the MASIE regions, as is the case with the results in Figure 9. However, unlike the  
 466 break-up start date, the break-up end date also occurs later at Mestersvig than for the Greenland  
 467 Sea MASIE region. The opposite relationship is found in the Kara Sea / Sabetta and the  
 468 Chukchi Sea (Bering Strait), where the MASIE region has the earlier break-up end date. The  
 469 temporal trends in the break-up end dates are generally similar for the coastal locations and  
 470 the MASIE regions, and there are no differences in sign. All coastal locations and all MASIE  
 471 regions show negative trends, i.e., trends toward earlier break-up end dates in recent decades.

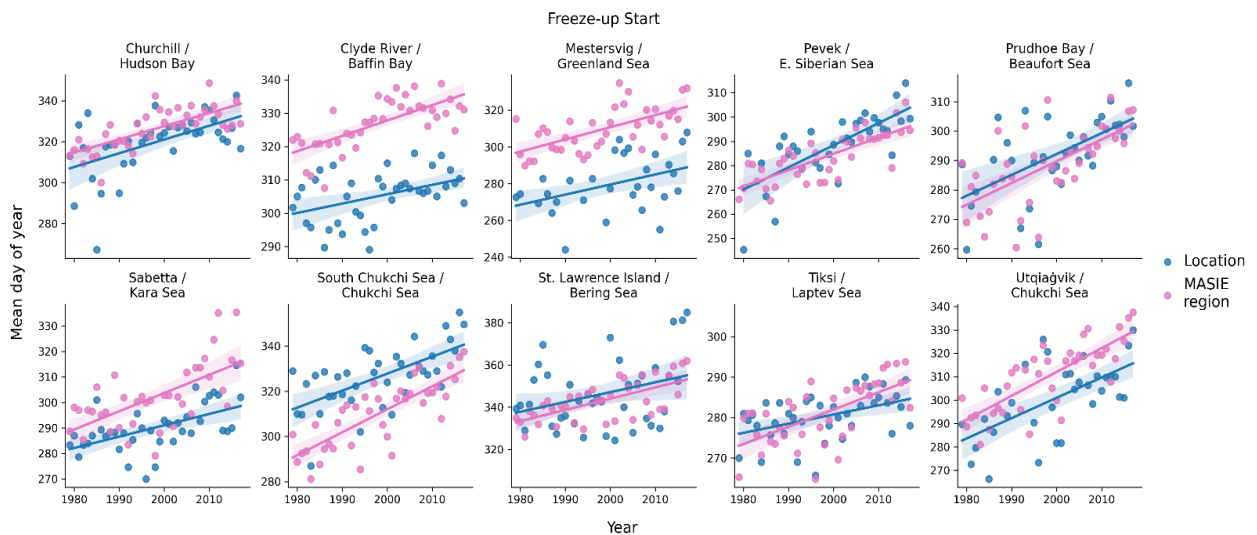


472

473 Figure 10. Yearly values (1979-2018) of the break-up end dates (shown as day-of-the-year  
 474 numbers) for the coastal locations (blue) and the corresponding MASIE regions (pink). Date  
 475 scales on y-axis vary among panels in order to optimize display of data points. Linear  
 476 regression lines are shown with the same color coding. In each panel, the upper line of header  
 477 identifies the coastal location and the lower line identifies the MASIE region. All values are  
 478 based on the modified J&E algorithms. Slopes and significance levels are listed in Tables S2  
 479 and S3.

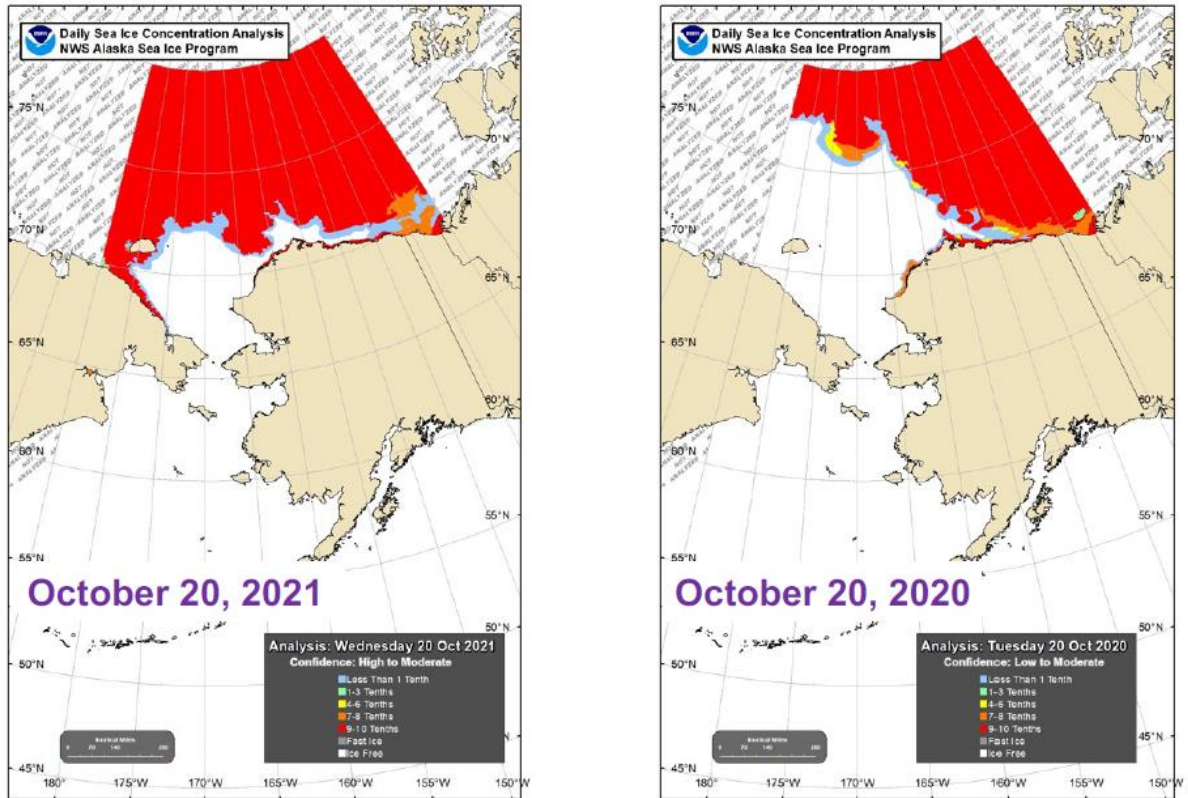
480 The freeze-up start dates are compared in Figure 11. Several regions show large offsets, most  
 481 notably Clyde River (Baffin Bay) and Mestersvig (Greenland Sea), where the start of freeze-  
 482 up occurs earlier at the coast by several weeks. Both Baffin Bay and the Greenland Sea are  
 483 large MASIE regions (Figure 2), favoring the delay of freeze-up start over a substantial  
 484 portion of the seasonal sea ice zone within the respective MASIE regions. Freeze-up start  
 485 dates are also earlier than offshore at several other coastal locations: Churchill, Sabetta and  
 486 Utqiagvik. These are regions in which it is common for ice to form along the coast in autumn,  
 487 with the ice edge advancing offshore to meet the expanding main ice pack as freeze-up

488 progresses. Figure 12 shows examples of this dual advance of the freeze-up “front” along the  
 489 coasts of the East Siberian Sea in 2021 and the Beaufort Sea in 2020 and 2021. By contrast,  
 490 the southern Chukchi Sea location has a later freeze-up date than the Chukchi MASIE region,  
 491 largely because the southern Chukchi grid cells are located in an area of relatively warm  
 492 inflowing currents from the Bering Sea and are in the southern portion of the Chukchi MASIE  
 493 region. As with the break-up end dates, all coastal locations and MASIE regions show trends  
 494 of the same sign. In this case, the trends are all positive, indicating a later start to freeze-up.



495  
 496 Figure 11. Yearly values (1979-2018) of the freeze-up start dates (shown as day-of-the-year  
 497 numbers) for the coastal locations (blue) and the corresponding MASIE regions (pink). Date  
 498 scales on y-axis vary among panels in order to optimize display of data points. Linear  
 499 regression lines are shown with the same color coding. In each panel, the upper line of header  
 500 identifies the coastal location and the lower line lists the MASIE region. All values are based  
 501 on the modified J&E algorithms. See Tables S2 and S3 for slopes and significance levels.

502



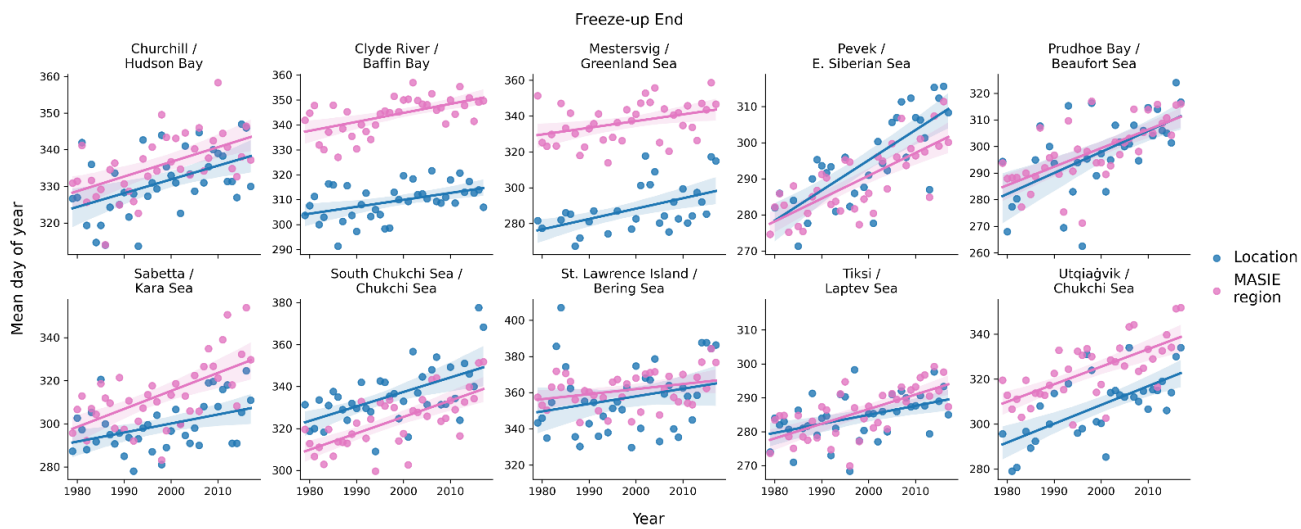
503

504 Figure 12. Sea ice coverage on October 20, 2021 (left panel) and October 20, 2020 (right  
 505 panel). As indicated by legends in lower right of each panel, red denotes essentially complete  
 506 ice coverage, while gray areas have low concentrations. Source: NWS Alaska Region Sea  
 507 Ice Desk.

508

509 Finally, Figure 13 compares the freeze-up end dates for the ten coastal sites and their MASIE  
 510 regions. The results are quite similar to those for the freeze-up start dates in Figure 11.  
 511 Relative to the MASIE regions as a whole, freeze-up ends earlier at both Canadian sites  
 512 (Churchill and Clyde River), Mestersvig, Sabetta and Utqiaġvik. Again, the differences are  
 513 especially large (more than a month) at Clyde River and Mestersvig, both of which are in  
 514 large MASIE regions as noted above. The southern Chukchi Sea and, to a lesser extent in

515 recent decades, Pevek (East Siberian Sea) show later freeze-ups near the coast than for the  
 516 MASIE region. Once again, all trends are positive, pointing to a later end to freeze-up at  
 517 coastal as well as offshore regions throughout the Arctic. The changes in the freeze-up dates  
 518 over the 40-year period are especially large, exceeding one month, at Pevek (East Siberian  
 519 Sea) and Prudhoe (Beaufort Sea). The changes are close to a month at Utqiaġvik (Chukchi  
 520 Sea) and the Southern Chukchi Sea.



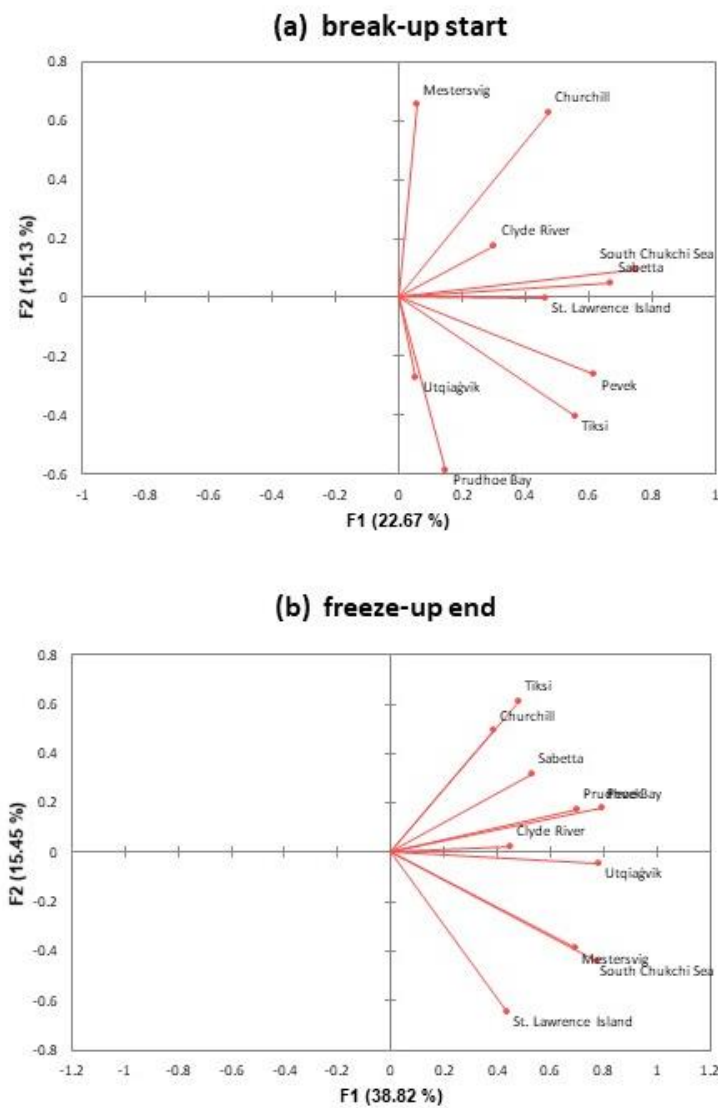
521  
 522 Figure 13. Yearly values (1979-2018) of the freeze-up dates (shown as day-of-the-year  
 523 numbers) for the coastal locations (blue) and the corresponding MASIE regions (pink). Date  
 524 scales on y-axis vary among panels in order to optimize display of data points. Linear  
 525 regression lines are shown with the same color coding. In each panel, the upper line of header  
 526 identifies the coastal location and the lower line identifies the MASIE region. All values are  
 527 based on the modified J&E algorithms. Slopes and their significance levels are listed in Tables  
 528 S2 and S3.

529 In order to synthesize the information provided by the local indicators, we applied a factor  
530 analysis to each of the four local indicators described in Section 2. For the local indicators,  
531 each input matrix was 10 (locations) x 40 (years). For comparison, we also applied the factor  
532 analysis to the corresponding regional sea ice areas from the MASIE database (National Snow  
533 and Ice Data Center dataset G02135\_v3.0-4). Because the Chukchi Sea is the MASIE region  
534 for two of the local indicators (Chukchi Sea and Utqiagvik), the data matrix for the MASIE  
535 regional factor analysis contained 9 (regions) x 40 (years) entries. We performed the MASIE  
536 factors separately for middle months of the break-up and freeze-up seasons (June and  
537 November, respectively).

538 In all cases, the first factor contains loadings of the same sign for all locations/regions and is  
539 essentially a depiction of the temporal trends, which account for substantial percentages of the  
540 variance. The second factor consists of loadings of both signs, corresponding to positive  
541 departures from the mean at some locations and negative departures at others. Figure 14  
542 illustrates this behavior for (a) the break-up start dates and (b) the freeze-up end dates. While  
543 every one of the ten locations has a positive loading in Factor 1, the mixed signs of the Factor  
544 2 loadings point to a regional clustering of the dates. For example, Figure 14a shows that the  
545 northern coastal sites in the Pacific hemisphere from 90°E eastward to 90°W (Prudhoe Bay,  
546 Utqiagvik, Tiksi, Pevek) have a component of break-up start date variability that is out of  
547 phase with the locations in the western Atlantic/eastern Canada sector from 90°W eastward to  
548 90°E (Mestersvig, Churchill, Clyde River).

549 The interpretation of Factor 1 as a trend mode is supported by Figure 15, which shows the  
550 time series of the scores of Factor 1 for (a) the break-up start date and (b) freeze-up end dates.  
551 The trends towards an earlier start of break-up and a later end of freeze-up are clearly evident.

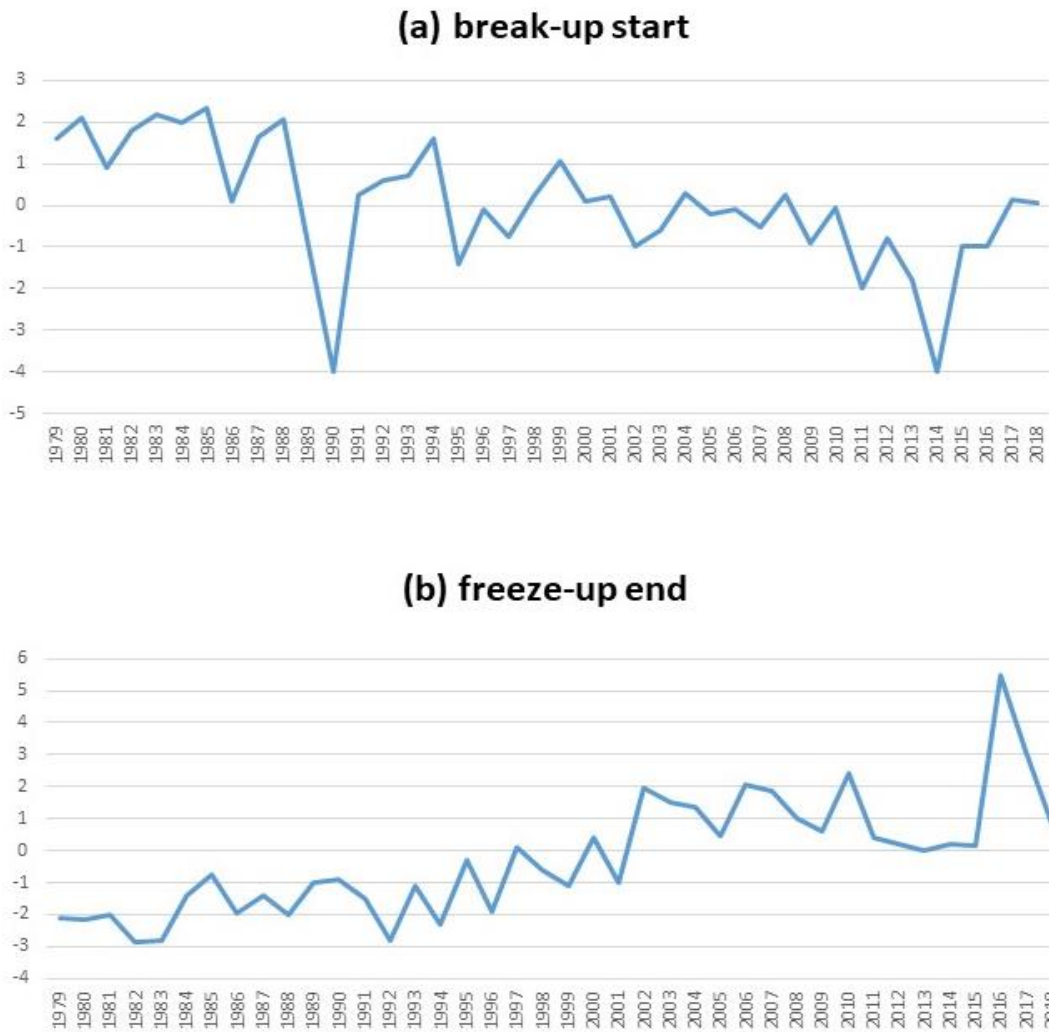
552 Figure 15 also illustrates the tendency for occasional “outlier” years to be followed by a  
 553 recovery in the following year. These plots and those for the other local indicators show that  
 554 these extreme excursions and recoveries are superimposed on the strong underlying trends,  
 555 resulting in new extremes when the sign of an extreme year is the same as the sign of the  
 556 underlying trend.



557

558 Figure 14. Loadings for Factor 1 (x-axis) and Factor 2 (y-axis) for (a) the start of break-up and (b)  
 559 the end of freeze-up at the ten local coastal sites. Labels on vectors denote locations.





560

561 Figure 15. Scores (time series) for Factor 1 of (a) the start of break-up and (b) the end of  
 562 freeze-up at the ten local coastal sites.

563 Table 4 shows that the first two factors explained more than half the variance for all local and  
 564 MASIE indicators except the local break-up start date. The break-up start date is notable for  
 565 the small percentages of variance explained by the first two factors. The implication is that  
 566 local conditions play a relatively greater role in the timing of the start of break-up. These local  
 567 factors can include landfast ice, inflow of water and heat from the adjacent land areas  
 568 (including rivers), and possibly other effects related to local ocean currents or local weather

569 conditions. The freeze-up start date has the most spatial coherence in the trend mode (55.7%  
570 of the explained variance). However, as shown by the last two lines of Table 4, the MASIE  
571 regional ice areas have even greater percentages of variance explained by the first two factors.  
572 In both the break-up and freeze-up seasons (June and November), the first two factors explain  
573 more than 60% of the variance (vs. 37.8%-55.7% for the local indicators). Because the  
574 variance of the ice concentrations in the MASIE regions is generally greater in the southern  
575 compared to the northern portion of the region, factors for individual MASIE regions have  
576 greater loadings in the south. However, this does not provide an obvious explanation for why  
577 the percentage of variance explained by the first factor is greater for the MASIE indicators  
578 than for the local indicators. These differences again point to the importance of local  
579 conditions relative to the broader underlying trend in ice coverage, as Factor 1 (the trend)  
580 accounts for most of the differences between the local and regional results in Table 4.

581

582 Table 4. Percentages of variance explained by Factors 1 and 2. Numbers in parentheses are  
583 the contributions of the individual factors (Factor 1 + Factor 2).

584

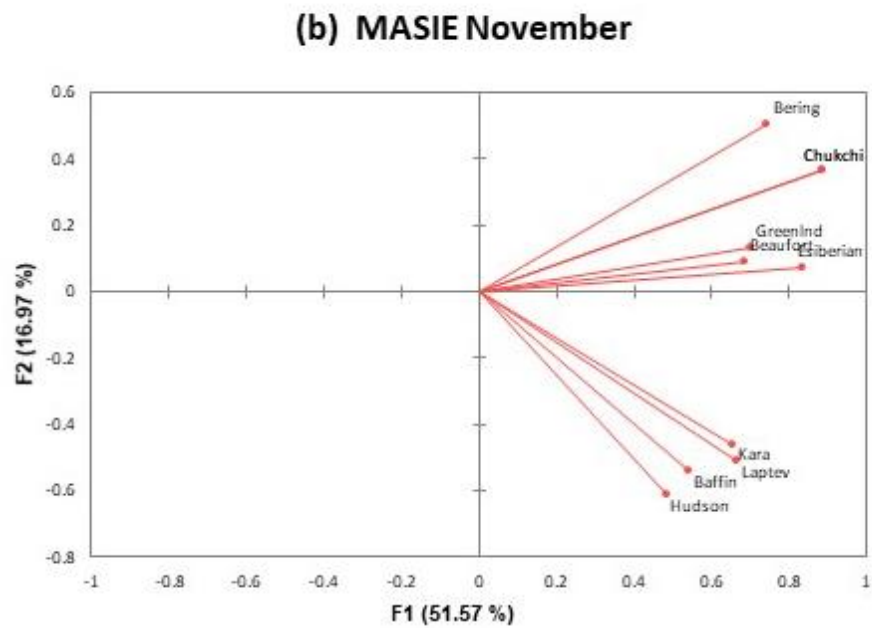
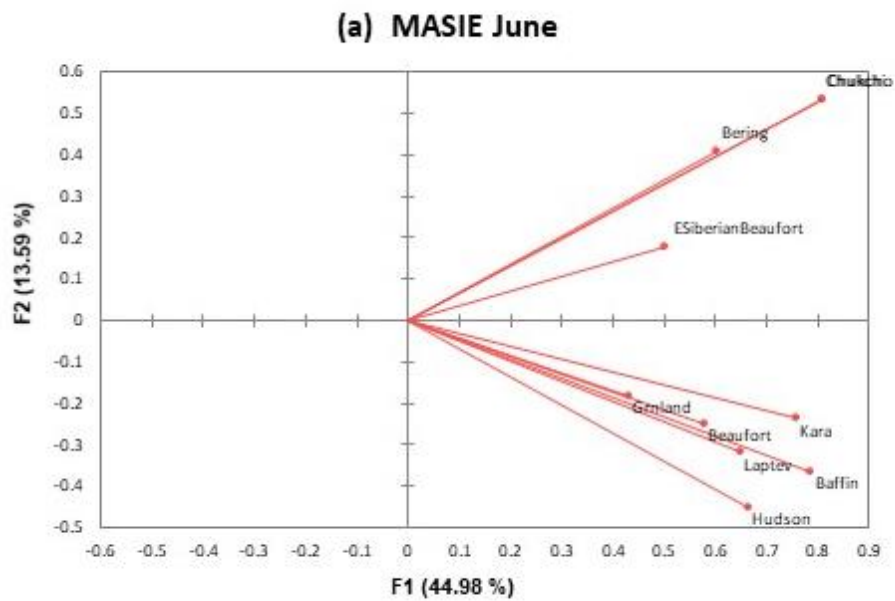
585	Break-up start (local)	37.8%	(22.7% + 15.1%)
586	Break-up end (local)	50.9%	(37.6% + 13.3%)
587	Freeze-up start (local)	55.7%	(40.1% + 15.6%)
588	Freeze-up end (local)	54.3%	(38.8% + 15.5%)
589			
590	MASIE ice areas: June	60.9%	(47.1% + 13.8%)
591	MASIE ice areas: November	64.1%	(48.7% + 15.4%)

592

593 Finally, Figure 16 illustrates the tendency for tighter clustering in the regional indicators. For  
594 both the June and November results, the clustering in Figure 16 is clearly more distinct than in  
595 Figure 14, which is the corresponding figure for the local indicators. The clustering in Figure  
596 16 is geographically coherent, e.g., the Pacific sector sites (Bering, Chukchi, East Siberian)  
597 are in a distinct cluster for the June (break-up), while subclusters for November include the  
598 Hudson and Baffin regions, the Kara and Laptev regions, and the Bering and Chukchi regions.  
599 The results imply that underlying trends and spatially coherent patterns of forcing will be  
600 more useful in explaining – and ultimately predicting – variations of regional sea ice cover.  
601 However, diagnosis and prediction of local indicators will require a greater reliance on  
602 additional information such as local geography and local knowledge, including information  
603 from residents and other stakeholders who have had experience with break-up and freeze-up  
604 of sea ice in the immediate area.

605

606



607

608 Figure 16. Loadings for Factor 1 (x-axis) and Factor 2 (y-axis) for the MASIE regional ice  
 609 areas of (a) June and (b) November. Labels on vectors denote MASIE regiona.

610

611 **4. Discussion**

612 The results presented in Section 3 point to a lengthening of the open water season as a result  
613 of both an earlier break-up and a later freeze-up. The timing of break-up and freeze-up differs  
614 between the coastal sites and the broader MASIE regions that are centered farther from shore  
615 than the coastal grid cells. These differences can be related to the presence of landfast ice,  
616 which characterizes the nearshore coastal waters to varying degrees at most of our coastal  
617 sites (Figure 1).

618 Landfast ice generally persists longer than pack ice in the adjacent offshore in spring. This  
619 contrast can be explained largely in terms of the stationary nature of the landfast ice cover,  
620 with grounded pressure ridges and confinement by coastal barrier islands (e.g., in the Beaufort  
621 and Kara Seas) locking the ice cover in place. Differences in ice thickness, with offshore sea  
622 ice younger and hence thinner in areas of coastal polynyas with winter new-ice formation  
623 (e.g., in the Chukchi, Beaufort and Laptev Seas) may also contribute to longer persistence of  
624 landfast ice. Finally, with thermal decay of sea ice as a key break-up mode, the absorption of  
625 solar shortwave energy in leads and openings in the offshore ice pack promotes thinning and  
626 decay of the offshore ice relative to that of the landfast ice. The latter is mostly lacking such  
627 areas of open water, rendering lateral melt and ocean-to-ice heat transfer from subsurface  
628 ocean heat storage less effective (see also Petrich et al., 2012).

629 Table 5 summarizes the coastal-MASIE differences in break-up dates by grouping the sites  
630 according to the role played by landfast ice. For several sites, the categorization of the landfast  
631 ice requires clarification. The Chukchi Sea location is a non-coastal site and therefore clearly  
632 beyond the extent of landfast ice (Figure 1). The St. Lawrence Island grid cells used here are  
633 considered to be unaffected by landfast ice because of their location southeast of the island, as

634 described in Section 2. The grid cells representing the Mestersvig region are located in the  
 635 coastal Greenland Sea, just outside of King Oscar Fjord. This region experiences dynamic ice  
 636 conditions with a comparatively short landfast ice season and a narrower landfast ice belt,  
 637 with ocean swell and ice pack interaction constraining extent and duration of the landfast ice  
 638 cover (Wadhams, 1981). For this reason, Mestersvig is listed below the other sites affected by  
 639 landfast ice in Table 5. With these caveats, it apparent from Table 5 that there is a general  
 640 tendency for later break-up (both the start and end dates) at locations affected by landfast ice.  
 641 The delay of the break-up ranges from about 5 to 40 days. Exceptions are Pevek and Sabetta,  
 642 where local freshwater inflows from streams and snowmelt may contribute to earlier break-  
 643 ups relative to the broader MASIE regions – a hypothesis that should be tested in future  
 644 research. There is no clear signal of earlier or later coastal break-up at Mestersvig and St.  
 645 Lawrence Island, where landfast ice is not a major contributor to the timing of break-up. The  
 646 earlier local break-up at the Chukchi site is primarily a function of its location in the southern  
 647 portion of the Chukchi MASIE region.

648 Table 5. Summary of landfast ice presence at each coastal site and timing of break-up at the  
 649 site relative to break-up in corresponding MASIE region (Figures 10 and 11).

650		<u>Landfast ice?</u>	<u>Break-up start (vs. MASIE)</u>	<u>Break-up end (vs. MASIE)</u>
651	Churchill	yes	later (~20 days)	similar
652	Clyde River	yes	later (~10 days)	later (~40 days)
653	Prudhoe Bay	yes	later (~15 days)	later (~15 days)
654	Utqiagvik	yes	later (~10 days)	later (~15 days)

655	Tiksi	yes	later (~15 days)	similar
656	Pevek	yes	earlier (~5 days)	earlier (~5 days)
657	Sabetta	yes	similar	earlier (~15 days)
658	Mestersvig	(yes)	earlier (~20 days)	later (~15 days)
659	St. Lawrence I.	no	earlier (~5 days)	similar
660	Chukcbi Sea	no	earlier (~10 days)	earlier (~35 days)

661

662 In the autumn, water in the shallow coastal areas cools more rapidly to the freezing point  
663 because there is less stored heat below the surface. Coastal waters can also be fresher than  
664 offshore waters because of terrestrial runoff that freshens the nearshore areas during the warm  
665 season. Under such conditions both a higher freezing point and reduction of convective  
666 overturning promote earlier freeze-up (Dmitrenko et al., 1999). As a result, the autumn freeze-  
667 up often proceeds outward from the coast as well as shoreward from the main pack ice (Figure  
668 12). However, onset of freeze-up – and depending on the geographic setting and offshore  
669 ocean and atmosphere conditions potentially also end of freeze-up – do not correspond with  
670 onset of landfast ice formation. In the Chukchi and Beaufort Sea, first appearance of landfast  
671 ice may lag freeze onset by a couple of weeks to three months (Mahoney et al., 2014). In more  
672 sheltered and less dynamic environments such as the Laptev Sea, inshore landfast ice typically  
673 does not form for another couple of weeks after onset of freeze-up and generally takes more  
674 than a month to extend further offshore (Selyuzhenok et al., 2015). Hence, freeze-up

675 variability and trends reported in this study are seen as largely independent of landfast ice  
676 processes.

677 Conversely, timing of freeze-up does impact the seasonal evolution of landfast ice. Mahoney  
678 et al. (2007) discuss mean climatology of annual landfast ice from 1996-2004, including  
679 analyses of the maximum, minimum and mean extents. Notable for the results presented in  
680 the present study is Mahoney et al.'s finding of a reduced presence of landfast ice in Beaufort-  
681 Chukchi region, due to later formation and earlier breakup. In a follow-up study, Mahoney et  
682 al. (2014) addressed the geographical variability of break-up and freeze-up, especially as it  
683 relates to landfast ice. Their results show that landfast ice in the central and western Beaufort  
684 Sea forms earlier, breaks up later, occupies deeper water and extends further from shore than  
685 that in the Chukchi Sea. These differences are partially due to the orientation of the coastline  
686 relative to the prevailing easterly winds, which can more readily advect ice away from the  
687 southwest-northeast oriented coastline of the Chukchi Sea. Hosekova et al. (2021) examined  
688 landfast ice along the northern Alaska coast in the context of the buffering of the coastline  
689 from wave activity. They found that the wave attenuation by landfast ice was weaker in  
690 autumn than in spring because of the lower ice thickness in autumn compared to spring.  
691 However, the importance of waves for breakup is somewhat limited because it typically  
692 requires large fetch with does not develop until later in the summer and fall, well past the end  
693 of break-up season.

694 Yu et al. (2014) showed that landfast ice has large interannual variations, which imply large  
695 variations in break-up and freeze-up. Superimposed on these variations were notable trends in  
696 landfast ice during Yu et al's study period, 1976-2007. More specifically, the duration of  
697 landfast ice was found to have shortened in the Chukchi, East Siberian and Laptev Seas,



698 primarily as a result of a slower offshore expansion of landfast ice during the autumn and  
699 early sinter since 1990. Our coastal sites in these sectors (Utqiagvik, Pevek and Tiksi) show  
700 notable trends toward earlier break-up and later freeze-up, consistent with Yu et al.'s (2014)  
701 trends in landfast ice.

702  
703 Cooley et al. (2020) examined the sensitivity of landfast ice break-up at the community level  
704 in the Canadian Arctic and western Greenland to temperature variations and trends based on  
705 analysis of visible satellite imagery. Our analysis provides a longer reference period (40 years  
706 vs. 19 years) and a broader geographical context for the work by Cooley and collaborators.

707 Cooley et al. (2020) also used the relationships between air temperature and landfast ice  
708 break-up date, together with projected changes in air temperature from a set of eight CMIP5  
709 global climate models, to project future changes in the breakup dates. Specifically, we note  
710 that the trends projected for the remainder of the century in Cooley et al. (2020) are in many  
711 instances less pronounced (in days/decade shift in breakup) than those identified here. For  
712 example, for Clyde River Cooley et al. project a shift in breakup to an earlier date by 23 days  
713 by the year 2099 as compared to changes of a similar magnitude but over a much shorter time  
714 period examined here (Fig. 9 and 10). For Clyde River, the comparison between trends in the  
715 local break-up timing compared to that for the broader region (Baffin Bay) also reveals that  
716 the regional trends are much less pronounced than those at the local scale (Fig. 9 and 10).

717 Furthermore, the two westernmost communities examined by Cooley et al. (2020),  
718 Tuktoyaktuk and Paulatuk (Eastern Beaufort Sea), were projected to see earlier landfast ice  
719 break-up onset of 5 days and 11 days, respectively, by 2099. The data compiled here for  
720 Prudhoe Bay and the Beaufort Sea indicate a substantially larger shift towards earlier dates by  
721 more than 5 days *per decade* (Fig. 9 and 10).

722 One other study that addressed future changes of sea ice duration in the Pacific sector of the  
723 Arctic is Wang et al.'s (2018) evaluation mid-21<sup>st</sup>-century projections based on sea ice  
724 concentrations simulated by seven CMIP5 global climate models. However, Wang et al.'s  
725 evaluations were for the broader offshore areas of the East Siberian, Chukchi and Beaufort  
726 Seas rather than for immediate coastal areas, as global climate models generally do not  
727 include landfast ice. Pan-Arctic models that simulated landfast ice parameterized  
728 thermodynamically without addressing its mobility had significant problems in forecasting  
729 coastal ice thickness, especially during freeze-up in September and October (Johnson et al.,  
730 2012). The projected increases in ice-free season length over the 2015-2044 period were  
731 found were found to vary from about 20 days in the Bering Strait region to up to 60 days in  
732 the offshore areas of the East Siberian, Chukchi and Beaufort Seas. While these changes are  
733 for offshore areas, they are larger than those projected for coastal areas by late century in the  
734 study of Cooley et al. (2020). .

## 735 **5. Conclusion**

736 The primary objective of this study was to use the locally-based metrics to construct  
737 indicators of break-up and freeze-up at near-coastal locations in which sea ice has high  
738 stakeholder relevance. A set of ten coastal locations distributed around the Arctic were  
739 selected for this purpose. The sea ice indicators used here are based on local ice climatologies  
740 informed by community ice use (Johnson and Eicken, 2016; Eicken et al., 2014) rather than  
741 prescribed "universal" thresholds of ice concentration (e.g., 15%, 80%) used in other recent  
742 studies of sea ice break-up and freeze-up.

743 The trends and interannual variations of the local indicators of break-up and freeze-up at the  
744 ten nearshore are similar to the trends and variations of corresponding indicators for broader  
745 offshore regions, but the site-specific indicators often differ from the regional indicators by  
746 several days to several weeks. Relative to indicators for broader adjacent seas, the coastal  
747 indicators show later break-up at sites known to have extensive landfast ice, whose break-up  
748 typically lags retreat of the adjacent, thinner drifting ice. The coastal indicators also show an  
749 earlier freeze-up at some sites in comparison with freeze-up for broader offshore regions,  
750 likely tied to earlier freezing of shallow water regions and areas affected by freshwater input  
751 from nearby streams and rivers. However, the trends towards earlier break-up and later freeze-  
752 up are unmistakable over the post-1979 period at nearly all the coastal sites and their  
753 corresponding regional seas.

754 The coastal indicators of the seasonal ice cycle for this study are based on Alaskan ice users.  
755 However, ice uses and ice hazards in this region, as reflected in the definition of key seasonal  
756 indicators, align with those of other coastal regions in the Arctic. Specifically, the  
757 commonalities between coastal populations using the sea ice cover (both drifting and landfast)  
758 as a platform for a range of activities, and to whom sea ice poses a hazard for boating and  
759 marine vessel traffic, justify the approach taken in this study to extrapolate from the Alaskan  
760 Arctic (with a range of ice conditions representative of the broader Arctic) to the pan-Arctic  
761 scale.

762 The differences between the coastal and offshore regional indicators matter greatly to local  
763 users whose harvesting of coastal resources and Indigenous culture are closely tied to the  
764 timing of key events in the seasonal ice cycle (Huntington et al., 2021; Eicken et al., 2014).  
765 These differences also matter from the perspective of maritime activities, where access to

766 coastal locations for destination traffic is a key factor (Brigham, 2017). These offsets vary  
767 considerably by region. In light of these findings, we view locally as well as regionally  
768 defined measures of sea-ice break-up and freeze-up as a key set of indicators linking pan-  
769 Arctic or global indicators such as sea-ice extent or volume to local and regional uses of sea  
770 ice, with the potential to inform community-scale adaptation and response. We thank the two  
771 reviewers for their constructive comments and careful reading of the manuscript.

## 772 **Acknowledgments**

773 This work was supported by the Climate Program Office of the National Oceanic and  
774 Atmospheric Administration through Grant NA17OAR431060. Additional funding was  
775 provided by the Interdisciplinary Research for Arctic Coastal Environments (InterFACE)  
776 project through the U.S. Department of Energy, Office of Science, Biological and  
777 Environmental Research RGMA program.

## 778 **Data Availability**

779 The daily grids of passive-microwave-derived sea ice concentrations are available from the  
780 National Snow and Ice Data Center as dataset NSIDC-0051, available at  
781 <https://nsidc.org/data/nsidc-0051>. Lists of the indicator dates for the coastal sites and the  
782 MASIE regions are available from the author on request.

## 783 **Author contributions**

784 JEW served the principal investigator for the study, led the drafting of the manuscript, and  
785 performed the factor analysis described in Section 3. HE supervised the implementation of  
786 the revised indicators for the coastal sites and the MASIE regions, and drafted parts of the

787 text. KR performed the indicator calculations, produced Figures 1-11, and assisted in the  
788 preparation of the manuscript. MJ designed the original indicators, participated in the  
789 modification of the indicators, and contributed to the revision of the manuscript.

## 790 **Competing interests**

791 The authors declare that they have no conflict of interest

## 792 **References**

793 AMAP: Adaptation Actions for a Changing Arctic: Perspectives from the Baffin Bay/Davis  
794 Strait Region. Arctic Monitoring and Assessment Programme (AMAP), Oslo, Norway. xvi +  
795 354 pp, <https://www.amap.no/documents/download/3015/inline>, 2018.

796 AMAP: Snow, water, ice and permafrost in the Arctic (SWIPA) 2017, Arctic Monitoring and  
797 Assessment Programme (AMAP), Oslo, Norway, xiv + 269 pp. 2017.

798

799 Bliss, A.C., and Anderson, M.R.: Arctic sea ice melt onset and timing from passive  
800 microwave- and surface air temperature-based methods, *J. Geophys. Res.*, 123, 9063-9080,  
801 <https://doi.org/10.1029/2018JD028676>, 2018.

802

803 Bliss, A.C., Steele, M., Peng, G., Meier, W.M., and Dickinson, S: Regional variability of  
804 Arctic sea ice seasonal climate change indicators from a passive microwave climate data  
805 record, *Environ. Res. Lett.*, 14, 045003, <https://doi.org/10.1088/1748-9326/aafb84>, 2019.

806

807 Box, J.E., and 19 coauthors: Key indicators of Arctic climate change: 1971–2017, *Environ..*  
808 *Res. Lett.*, 14(4),.045010, <https://doi.org/10.1088/1748-9326/aafc1b>, 2019.

809

810 Brigham, L.W.: The changing maritime Arctic and new marine operations. In: Beckman, R.  
811 C., Henriksen, T., Dalaker Kraabel, K., Molenaar, E. J., and Roach, J. A. (eds.): *Governance*  
812 *of Arctic shipping* (pp. 1-23), Brill Nijhoff, 2017.

813

814 Cavalieri, D.J., Gloersen, P., and Campbell, W.J.: Determination of sea ice parameters with  
815 the NIMBUS-7 SMMR, *J. Geophys. Res.*, 89(D4): 5355-5369,  
816 <https://doi.org/10.1029/JD089iD04p05355>, 1984.

817

818 Cooley, S.W., Ryan, J.C., Smith, L.C., Horvat, C., Pearson, B., Dale, B. and Lynch, A.H.:  
819 Coldest Canadian Arctic communities face greatest reductions in shorefast sea ice. *Nature*  
820 *Climate Change*, 10(6), pp.533-538.

821 <https://www.nature.com/articles/s41558-020-0757-5>, 2020.

822

823 Dammann, D.O., Eicken, H., Mahoney, A.R., Meyer, F.J. and Betcher, S: Assessing sea ice  
824 trafficability in a changing Arctic. *Arctic*, 71(1), 59-75, <https://doi.org/10.14430/arctic4701>,  
825 2018.

826

827 Deser, C., Walsh, J.E., and Timlin, M.S.: Arctic sea ice variability in the context of recent  
828 atmospheric circulation trends, *J. Climate*, 13, 617-633, [https://doi.org/10.1175/1520-  
829 0442\(2000\)013<0617:ASIVIT>2.0.CO;2](https://doi.org/10.1175/1520-0442(2000)013<0617:ASIVIT>2.0.CO;2), 2000.

830 Druckenmiller, M.L. et al.: The Arctic. *Bull. Amer. Meteor. Soc.*, 102, S263-S316,  
831 <https://doi.org/10.1175/BAMS-D-21-0086.1>, 2021.

832 Eicken, H., Kaufman, M., Krupnik, I., Pulsifer, P., Apangalook, L., Apangalook, P., Weyapuk  
833 Jr, W., and Leavitt, J.: A framework and database for community sea ice observations in a  
834 changing Arctic: An Alaskan prototype for multiple users, *Polar Geogr.*, 37(1), 5-27,  
835 <http://dx.doi.org/10.1080/1088937X.2013.873090>, 2014.

836

837 Fang, A., and Wallace, J. M.: Arctic sea ice variability on a timescale of weeks in relation to  
838 atmospheric forcing, *J. Climate*, 7, 1897-1914, [https://doi.org/10.1175/1520-  
839 0442\(1994\)007<1897:ASIVOA>2.0.CO;2](https://doi.org/10.1175/1520-0442(1994)007<1897:ASIVOA>2.0.CO;2), 1994. .

840

841 Fu, D., Liu, B., Yu, G., Huang, H., and Qu, L: Multiscale variations in Arctic sea ice motion  
842 and links to atmospheric and oceanic conditions, *The Cryosphere*, 15, 3797-3811,  
843 <https://doi.org/10.5194/tc-15-3797-2021>, 2021.

844

845 Hosekova, L., Eidam, E., Panteleev, G., Rainville, L., Rogers, W.E., and Thomson, J.:  
846 Landfast ice and coastal wave exposure in northern Alaska. *Geophys. Res. Lett.*, 48(22),  
847 e2021GL095103, <https://doi.org/10.1029/2021GL095103>, 2021.

848

849 Huntington, H. P., Raymond-Yakoubian, J., Noongwook, G., Naylor, N., Harris, C.,  
850 Harcharek, Q. and Adams, B.: “We never get stuck”: A collaborative analysis of change and  
851 coastal community subsistence practices in the northern Bering and Chukchi Seas,  
852 *Alaska, Arctic*, 74(2), 113-126, 2021.

853

854 IPCC: Climate Change 2021: The Physical Science Basis. Contribution of Working Group I  
855 to the Sixth Assessment Report of the Intergovernmental Panel on Climate Change [Masson-  
856 Delmotte, V., Zhai, P., Pirani, A., Connors, S. L., Péan, C., Berger, S., Caud, N., Chen, Y.,  
857 Goldfarb, L., Gomis, M. I., Huang, M., Leitzell, K. Lonnoy, E., Matthews, J. B. R., Maycock,  
858 T. K., Waterfield, Y., Yelekçi, O., Yu, R., and Zho, B. (eds.)]. Intergovernmental Panel on  
859 Climate Change, Cambridge University Press.  
860 [https://www.bing.com/search?FORM=AFSCVO&PC=AFSC&q=IPCC+AR6+Working+Gro  
861 up+1+report](https://www.bing.com/search?FORM=AFSCVO&PC=AFSC&q=IPCC+AR6+Working+Group+1+report), 2022.

862

863 Johnson, M., and Eicken, H.: Estimating Arctic sea-ice freeze-up and break-up from the  
864 satellite record: A comparison of different approaches in the Chukchi and Beaufort Seas,  
865 *Elementa: Science of the Anthropocene*, 4, 000124, doi:10.12952/journal.elementa.000124,  
866 2016.

867

868 Johnson, M., et al.: Evaluation of Arctic sea ice thickness simulated by Arctic Ocean Model  
869 Intercomparison Project models, *J. Geophys. Res.*, 117, C00D13, doi:10.1029/2011JC007257,  
870 2012

871

872 Kapsch, M.L., Eicken, H., and Robards, M.: Sea ice distribution and ice use by indigenous  
873 walrus hunters on St. Lawrence Island, Alaska. In *SIKU: Knowing Our Ice* (Krupnik, I.,  
874 Aporta, C., Gearheard, S., Laidler, G. J., and Lielsen Holm, L., Eds.), 115-144, Springer,  
875 Dordrecht, 2010.

876

877 Krupnik, I., Apangalook, L., and Apangalook, P: “It’s cold, but not cold enough”: Observing  
878 ice and climate change in Gambell, Alaska, in *IPY 2007-2008 and beyond*. In *SIKU:  
879 Knowing Our Ice* (Krupnik, I., Aporta, C., Gearheard, S., Laidler, G. J., and Lielsen Holm, L.,  
880 Eds.), 81-114, Springer, Dordrecht, 2010.

881

882 Mahoney, A.R., Eicken H., Gaylord A.G., and Gens R.: Landfast sea ice extent in the  
883 Chukchi and Beaufort Seas: The annual cycle and decadal variability. *Cold Reg. Sci.  
884 Technol.*, 103, 41–56. doi: 10.1016/j.coldregions.2014.03.0033, 2014..

885

886 Mahoney, A.R., Eicken, H., Gaylord, A.G., and Shapiro, L: Alaska landfast sea ice: Links  
887 with bathymetry and atmospheric circulation, *J. Geophys. Res.*, 112, C02001,  
888 doi:10.1029/2006JC003559, 2007.

889

890 Markus, T., Stroeve J. C., and Miller, J: Recent changes in Arctic sea ice melt onset, freezeup  
891 and melt season length, *J. Geophys. Res. (Oceans)*, 114, 1-14,  
892 <https://doi.org/10.1029/2009JC005436>, 2009.

893

894 Meier, W., Fetterer, F., Savoie, M., Mallory, S. Duerr, R., and Stroeve, J.: NOAA/NSIDC  
895 Climate Data Record of Passive Microwave Sea Ice Concentration, Version 3 (Boulder,  
896 Colorado USA; National Snow and Ice Data Center), <https://doi.org/10.7265/N59P2ZTG>,  
897 [Accessed 16 January 2022, 2017].

898

899 Noongwook, G.: Native Village of Savoonga, Native Village of Gambell. In Huntington,  
900 H.F., and George, J.C.: Traditional knowledge of the bowhead whale (*Balaena mysticetus*)  
901 around St. Lawrence Island Alaska, 47-54, 2007.

902

903 Onarheim, I.H., Eldevik, T., Smedsrud, L.H., and Stroeve, J.C.: Seasonal and regional  
904 manifestations of Arctic sea ice loss, *J. Climate*, 31, 4917-4932, [https://doi.org/10.1175/JCLI-](https://doi.org/10.1175/JCLI-D-17-0427.1)  
905 [D-17-0427.1](https://doi.org/10.1175/JCLI-D-17-0427.1), 2018.

906

907 Peng, G., Steele, M., Bliss, A. C., Meier, W. N., and Dickinson, S: Temporal means and  
908 variability of Arctic sea ice melt and freeze season climate indicators using a satellite climate  
909 data record, *Remote Sensing*, 10, 1328, <https://doi.org/10.3390/rs10091328>, 2018.

910

911 Petrich, C., Eicken, H., Zhang, J., Krieger, J., Fukamachi, Y., and Ohshima, K.J.: Coastal  
912 landfast sea ice decay and breakup in northern Alaska: Key processes and seasonal prediction,  
913 *J. Geophys. Res.*, 117, C02003, doi:10.1029/2011JC007339, 2012.

914  
915 Selyuzhenok, V., Krumpfen, T., Mahoney, A., Janout, M., and Gerdes, R.: Seasonal and  
916 interannual variability of fast ice extent in the southeastern Laptev Sea between 1999 and  
917 2013, *J. Geophys. Res. Oceans*, 120, 7791–7806, doi:10.1002/2015JC011135, 2015.  
918  
919 Smith, A., and Jahn, A.: Definition differences and internal variability affect the simulated  
920 Arctic sea ice melt season, *The Cryosphere*, 12, 1-20, <https://doi.org/10.5194/tc-13-1-2019>,  
921 2019.  
922  
923 Serreze, M.C., Crawford, A.D., Stroeve, J.C., Barrett, A.P. and Woodgate, R.A.: Variability,  
924 trends, and predictability of seasonal sea ice retreat and advance in the Chukchi Sea. *J.*  
925 *Geophys. Res. (Oceans)*, 127, 7308–7325, 2016.  
926  
927 Stammerjohn, S., Massom, R., Rind, D. and Martinson, D.: Regions of rapid sea ice change:  
928 an inter-hemispheric seasonal comparison. *Geophys. Res. Lett.* 39, L06501, 2017.  
929  
930 Stroeve, J.C., Crawford, A.D. and Stammerjohn, S.: Using timing of ice retreat to predict  
931 timing of fall freeze-up in the Arctic. *Geophys. Res. Lett.* 43, 6332–6340, 2016.  
932  
933 Stroeve, J.C., Markus, T., Boisvert, L., Miller, J., and Barrett, A.: Changes in Arctic melt  
934 season and implications for sea ice loss. *Geophys. Res. Lett.*, 41, 1216-1225,  
935 <https://doi.org/10.1002/2013GL058951>, 2014.  
936  
937 Stroeve, J., and Notz, D.: Changing state of Arctic sea ice across all seasons. *Env. Res. Lett.*,  
938 13, 102001, <https://doi.org/10.1088/1748-9326/aade56>, 2018.  
939  
940 Thomson, J., Smith, M., Drushka, K. and Lee, C.: Air-ice-ocean interactions and the delay of  
941 autumn freeze-up in the western Arctic Ocean. *Oceanography*,  
942 <https://doi.org/10.5670/oceanog.22.124>, 2022.  
943  
944 USGCRP: Climate Science Special Report: Fourth National Climate Assessment, Volume I  
945 (Wuebbles, D.J., Fahey, D.W., Hibbard, K.A., Dokken, D.J., Stewart, B.C., and Maycock,  
946 T.K.[eds.]). U.S. Global Change Research Program, Washington, DC, USA, 470 pp., doi:  
947 10.7930/J0J964J6, 2017  
  
948 Wadhams, P.: The ice cover in the Greenland and Norwegian Seas. *Reviews of Geophysics*  
949 and *Space Physics*, 19(3), 345–93, doi: [10.1029/RG019i003](https://doi.org/10.1029/RG019i003), 1981.  
  
950 Wang, M., Yang, Q., Overland, J.E., and Stabeno, P.: Sea-ice cover timing in the Pacific  
951 Arctic: The present and projections to mid-century by selected CMIP5 models. *Deep Sea*  
952 *Research Part II: Topical Studies in Oceanography*, 152, 22-34,  
953 <https://www.sciencedirect.com/science/article/pii/S0967064516302132>, 2018  
954  
955 Walsh, J. E., and Johnson, C. M.: Interannual atmospheric variability and associated  
956 fluctuations in Arctic sea ice extent, *J. Geophys. Res.*, 84, 6915–6928,  
957 <https://doi.org/10.1029/JC084iC11p06915>, 1979.



958 Yu, Y, Stern, H., Fowler, C., Fetterer, F., and Maslanik, J.: Interannual variability of Arctic  
959 landfast ice between 1976 and 2007. *J. Climate*, Vol. 27, 227-243, doi: [10.1175/JCLI-D-13-](https://doi.org/10.1175/JCLI-D-13-00178.1)  
960 [00178.1](https://doi.org/10.1175/JCLI-D-13-00178.1), 2014.